RESEARCH PAPER

Channels 6:3, 181-196; May/June 2012; © 2012 Landes Bioscience

Matrix metalloproteinase-9 and -2 enhance the ligand sensitivity of photoreceptor cyclic nucleotide-gated channels

Peter C. Meighan,[1] Starla E. Meighan,[1] Elizabeth D. Rich,[1] R. Lane Brown [1,2] and Michael D. Varnum [1,3,*]

[1]Department of Veterinary and Comparative Anatomy, Pharmacology and Physiology; Program in Neuroscience; Washington State University; Pullman, WA USA; [2]WWAMI Medical Education Program; Washington State University; Pullman, WA USA; [3]Center for Integrated Biotechnology; Washington State University; Pullman, WA USA

Keywords: cyclic nucleotide-gated channel, cone, rod, photoreceptor, extracellular protease, matrix metalloproteinase, gating

Abbreviations: CNG, cyclic nucleotide-gated; MMP, matrix metalloproteinase; ECM, extracellular matrix; cGMP, cyclic guanosine monophosphate; cAMP, cyclic adenosine monophosphate

Photoreceptor cyclic nucleotide-gated (CNG) channels are the principal ion channels responsible for transduction of the light-induced change in cGMP concentration into an electrical signal. The ligand sensitivity of photoreceptor CNG channels is subject to regulation by intracellular signaling effectors, including calcium-calmodulin, tyrosine kinases and phosphoinositides. Little is known, however, about regulation of channel activity by modification to extracellular regions of CNG channel subunits. Extracellular proteases MMP9 and -2 are present in the interphotoreceptor matrix adjacent to photoreceptor outer segments. Given that MMPs have been implicated in retinal dysfunction and degeneration, we hypothesized that MMP activity may alter the functional properties of photoreceptor CNG channels. For heterologously expressed rod and cone CNG channels, extracellular exposure to MMPs dramatically increased the apparent affinity for cGMP and the efficacy of cAMP. These changes to ligand sensitivity were not prevented by destabilization of the actin cytoskeleton or by disruption of integrin mediated cell adhesion, but could be attenuated by inhibition of MMP catalytic activity. MMP-mediated gating changes exhibited saturable kinetic properties consistent with enzymatic processing of the CNG channels. In addition, exposure to MMPs decreased the abundance of full-length expressed CNGA3 subunits, with a concomitant increase in putative degradation products. Similar gating effects and apparent proteolysis were observed also for native rod photoreceptor CNG channels. Furthermore, constitutive apparent proteolysis of retinal CNGA1 and retinal MMP9 levels were both elevated in aged mice compared with young mice. Together, these results provide evidence that MMP-mediated proteolysis can regulate the ligand sensitivity of CNG channels.

Introduction

Matrix metalloproteinases (MMPs) are a family of over 20 secreted and cell-surface, Zn^{2+}- and Ca^{2+}-dependent endopeptidases. MMPs are classically associated with tissue remodeling through proteolysis of extracellular matrix (ECM) and cell adhesion molecules. MMPs have been implicated in a variety of normal and abnormal processes throughout the body, such as embryological development, tumor growth and metastasis, wound healing, angiogenesis and vascular integrity and cyclical reproductive tissue remodeling.[1] More recently, MMPs have been shown to mediate normal and injury/disease-associated plasticity of excitable tissues. MMPs are necessary for activity-dependent plasticity within the hippocampus[2-7] and have been shown to mediate hippocampal-dependent learning.[8-10] Abnormal MMP expression has been linked to maladaptive form and function of excitable tissues and subsequent disease expression within the nervous system. MMP expression plays a critical role in stroke, traumatic brain injury and neurodegenerative disease.[11-15]

An emerging field is the role of MMPs in normal and disease processes within the retina. MMPs have been localized within several subcellular regions of the retina, including the interphotoreceptor matrix (IPM), and are thought to promote normal retinal function.[16-19] General retinal depolarization and exposure of the retina to visible light are both capable of inducing MMP expression in the retina.[20-22] MMPs are also thought to contribute to the progression of several retinal diseases, particularly those involving structural remodeling events.[23] Aberrant MMP regulation has been described in diabetic retinopathy,[24-26] age-related macular degeneration,[27-30] blood-retinal barrier breakdown,[25,28] retinal ischemia,[31] retinal rod degeneration in the rd1 mouse,[32] and retinal excitotoxicity.[20,21,33]

Although MMP function has been linked primarily to tissue remodeling and maintenance, MMPs also have been shown to influence ion channel and receptor function by direct proteolysis

*Correspondence to: Michael D. Varnum; Email: varnum@wsu.edu
Submitted: 05/11/12; Accepted: 05/28/12
http://dx.doi.org/10.4161/chan.20904

of core subunits. For example, MMP-7 cleaves the NR1 subunit of the NMDA receptor, altering the flux of Ca^{+2} in neuronal cells and decreasing the NMDA receptor contribution to hippocampal synaptic current.[34] MMP-3 is responsible for the removal of the extracellular glycine-binding epitope of the NMDA NR1 receptor subunit following prolonged NMDA receptor stimulation.[35] Additionally, a toxin-like domain within MMP-23 has been demonstrated to block K^+ channels.[36] Therefore, the role of MMPs extends beyond classical tissue remodeling.

The localization of MMPs to the IPM places them in proximity to extracellular and membrane bound structures associated with the photoreceptor outer segments, including CNG channels. Native CNG channels are hetero-tetrameric proteins composed of two structurally related subunit types: CNGA1 and CNGB1 in rod photoreceptors; CNGA3 and CNGB3 in cone photoreceptors.[37,38] Given that extracellular proteolysis has been shown to alter the gating properties and functional expression of other ion channels,[4,35,39] we hypothesized that MMPs may directly or indirectly influence CNG channel function. Here we report that the extracellular application of activated MMP9 dramatically modifies the gating of heterologously-expressed cone and rod CNG channels, as well as native amphibian rod CNG channels in excised patches. These gating effects appear to be a result of MMP-directed proteolysis of core channel subunits.

Results

MMP9 increases the ligand sensitivity of CNGA3 channels. To investigate the impact of MMP treatment on CNG channel function, we examined the effects of MMP9 exposure on CNGA3 homomeric channels. Inside-out patches excised from Xenopus oocytes expressing homomeric hCNGA3 were treated with recombinant human active MMP9 fragment. A low concentration of MMP9 (~10 nM) was added to the patch-electrode solution, such that access was limited to the extracellular surface of the membrane patch. We assessed CNG channel gating properties by measuring cGMP and cAMP dose-response curves and by determining the relative efficacy of cAMP, which is a partial agonist for CNGA3 channels at saturating ligand concentrations. Exposure to MMP9 for 60 min dramatically increased the current produced by 2 μM cGMP, a sub-saturating concentration of ligand (**Fig. 1A**). Dose-response relationships for channel activation by cGMP were obtained and fit with the Hill equation. The increased current elicited by sub-saturating cGMP resulted from an increased apparent affinity for cGMP (**Fig. 1B and C**), as MMP9 exposure effected an approximate 20-fold reduction in the $K_{1/2}$ cGMP compared with time-matched controls ($K_{1/2,GMP}$, mean ± SEM: $MMP9_{60\ min}$ = 0.62 μM ± 0.21; $control_{60\ min}$ = 12.6 μM ± 1.7; $p < 0.001$, Aspen-Welch t-test; n = 6). MMP9 also decreased the Hill slope (n_H) compared with control patches ($n_{H,cGMP}$: $MMP9_{60\ min}$ = 1.3 ± 0.1; $control_{60\ min}$ = 2.2 ± 0.2; $p < 0.001$, Student's t-test; n = 6). For control patches, a slight rundown (decrease) in cGMP sensitivity occurred, as previously described for oocyte-expressed cone CNG channels.[40] In addition, MMP9 increased both the efficacy of cAMP (I_{cAMP}/I_{MAX}: $MMP9_{60\ min}$ = 0.77 ± 0.05; $control_{60\ min}$ = 0.15 ± 0.05; $p < 0.001$, Student's t-test; n = 6; **Fig. 1D and E**) and the apparent affinity for cAMP ($K_{1/2,AMP}$: $MMP9_{80\ min}$ = 0.13 mM ± 0.04; $control_{80\ min}$ = 1.2 mM ± 0.09; $p < 0.01$, Student's t-test; n = 4) (**Fig. 1F and G**). The observed changes in channel ligand sensitivity were stable for the extent of the experiment (> 120 min). Longer time courses also revealed a decrease in maximum current, a finding that requires further characterization. Current-voltage relationships measured in a saturating concentration of cGMP (**Fig. 1H and I**) indicated that changes in channel gating were not accompanied by obvious alterations to channel voltage sensitivity or rectification ($I_{+100\ mV}/I_{-100\ mV}$: $MMP9_{initial}$ = 1.9 ± 0.1; $MMP9_{60\ min}$ = 2.0 ± 0.1; $p > 0.1$, paired t-test; n = 6). These results show that extracellular MMP9 can dramatically enhance the sensitivity of CNGA3 channels to activation by cGMP or cAMP.

To further characterize the MMP-associated increase in ligand sensitivity, we examined single channel activity of MMP9 treated CNGA3 channels. We observed that MMP9 treatment increased the open probability (P_O) during activation with sub-saturating concentrations of cGMP (**Fig. 2A and B**) (5 μM cGMP, $P_{O,t5}$ = 0.11, $P_{O,t30}$ = 0.43; 0.5 μM cGMP, $P_{O,t5} < 0.01$, $P_{O,t30}$ = 0.20). This finding is consistent with the increased macroscopic current amplitude at 2 μM cGMP (see **Fig. 1A**). Furthermore, we observed that exposure to MMP9 increased spontaneous channel openings in the absence of ligand (**Fig. 2C**) (0 cGMP, $P_{O,t5} < 0.01$, $P_{O,t30}$ = 0.06). Collectively, these data indicate that MMP9 alters the gating properties of CNGA3 channels.

Inhibition of MMP9 catalytic activity attenuates MMP9-induced gating effects. There are several possible mechanisms for the MMP-mediated effects on CNG channel gating, including: (1) direct binding of MMP9 or of MMP9-generated proteolytic fragments to the channel, thereby stabilizing the open state relative to the closed state; (2) direct proteolysis of the channel by MMP9, promoting channel opening; or (3) indirect signaling to the channel via other proteins and/or pathways. We determined whether the observed CNG channel gating effects required MMP catalytic activity using three distinct inhibition protocols. First, since MMP catalytic activity is dependent on association with divalent cations, including Zn^{2+} and Ca^{2+},[41] we controlled the free-divalent concentration of the extracellular (pipette) solution by modifying the concentration of chelator; divalent-cation chelators are commonly used as general inhibitors of MMP activity. Under these conditions, the rate of change in channel-gating parameters increased with the predicted amount of free divalents in the pipette solution (**Fig. 3A and B**). Varying the chelator concentration did not significantly alter gating in the absence of MMP9 (data not shown). Second, we coapplied MMP9 with a function-blocking antibody raised against the MMP9 catalytic region. The anti-MMP9 antibody significantly reduced the change in ligand sensitivity observed with MMP9 (**Fig. 3C**). Finally, we subjected MMP9 to denaturation by heating the MMP at 90°C for 1 h prior to patch-clamp recording. Similar to the other function-inhibiting treatments, heat inactivation of MMP9 substantially reduced the MMP9 associated gating effects (**Fig. 3C**). Taken together, these results demonstrate that MMP9 catalytic activity is necessary to produce the observed effects on CNG channel gating.

©2012 Landes Bioscience. Do not distribute

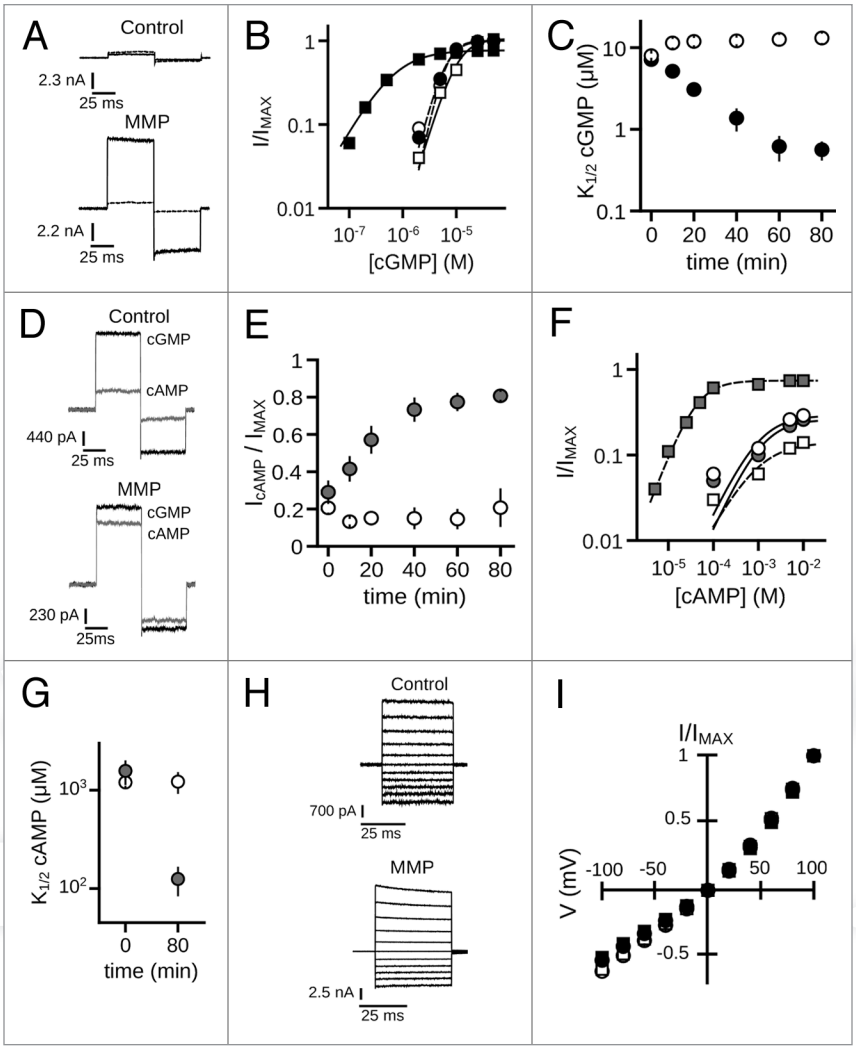

Figure 1. MMP9 increases the ligand sensitivity of CNGA3 homomeric channels. (A) Representative current traces from inside-out patches excised from Xenopus oocytes expressing homomeric human CNGA3 (A3) after activation by a sub-saturating concentration of cGMP (2 μM) for control (top) and ~10 nM MMP9-treated (bottom) patches immediately (t_0, dashed line) and 60 min (t_{60}, dark line) following excision. Current traces were elicited using voltage steps from a holding potential of 0 mV, to +80 mV, -80 mV and then returning to 0 mV. (B) Representative dose-response curves for activation of control (open symbols) and MMP9-treated (closed symbols) channels by cGMP at t_0 (circles) and t_{60} (squares). Currents were normalized to the maximum t_0 cGMP current. Continuous curves (t_0, hashed line; t_{60}, solid line) represent fits of the dose-response relationship to the Hill equation as indicated in Materials and Methods. Parameters for each condition shown are as follows: control, $K_{1/2,t0}$ = 6.6 μM, n_H = 2.9, I_{MAX} = 1.0, $K_{1/2,t60}$ = 10.3 μM, n_H = 2.1, I_{MAX} = 1.0; MMP9 $K_{1/2,t0}$ = 6.4 μM, n_H = 2.5, I_{MAX} = 1.0, $K_{1/2,t60}$ = 0.7 μM, n_H = 1.1, I_{MAX} = 0.8. (C) Time course for the change in cGMP apparent affinity for control (open circles) and MMP9-treated (filled circles) patches following excision. Data based on best fit Hill curves and expressed as mean $K_{1/2}$ (±SEM). (D) Representative current traces after activation by a saturating concentration of cGMP (1 mM, black line) or cAMP (10 mM, gray line) for control (top) and MMP9-treated (bottom) patches at 60 min following excision. (E) Time course for the change in cAMP efficacy for control (open circles) and MMP9-treated (filled circles) patches following excision. (F) Representative dose-response relationships for activation of control (open symbols) and MMP9 treated (closed symbols) A3 channels by cAMP at t_0 (circles) and t_{80} (squares). Currents were normalized to the maximum cGMP current. Parameters of best fit Hill curves (t_0, solid line; t_{80}, hashed line) for each condition shown are as follows: control, $K_{1/2,t0}$ = 1.0 mM, n_H = 1.1, I_{MAX} = 0.29, $K_{1/2,t80}$ = 0.9 mM, n_H = 1.0, I_{MAX} = 0.14; MMP9 $K_{1/2,t0}$ = 1.2 mM, n_H = 2.2, I_{MAX} = 0.26, $K_{1/2,t80}$ = 0.4 mM, n_H = 1.4, I_{MAX} = 0.74. (G) Summary of change in cAMP apparent affinity for control (open circles) and MMP9-treated (filled circles) patches. (H) Families of current traces elicited by voltage steps from -100 mV to +100 mV, recorded in the presence of 1 mM cGMP, for control (top) and MMP-treated (bottom) patches at 60 min following excision. (I) Mean (±SEM) current-voltage (I–V) relationships for control (open symbols) and MMP9-treated (filled symbols) patches at t_0 (circles) and t_{60} (squares). Scale bars

Proteolytic gating effects are not mediated by the actin cytoskeleton or integrin associated cell adhesion. Classically, MMP9 and MMP2 are associated with structural remodeling through degradation of extracellular matrix (ECM) molecules and modification of the pericellular environment. The physiologic effects of MMP activity often involve altering the activity of various cell adhesion molecules, notably integrins,[3,6,42,43] and by influencing cytoskeletal dynamics.[5,6,8] To investigate whether the observed MMP-dependent effects on CNG channel gating are mediated via cytoskeletal and/or integrin signaling modalities, we determined the effect of actin cytoskeleton disruption or interference of integrin/ECM interactions on the changes in $K_{1/2,GMP}$

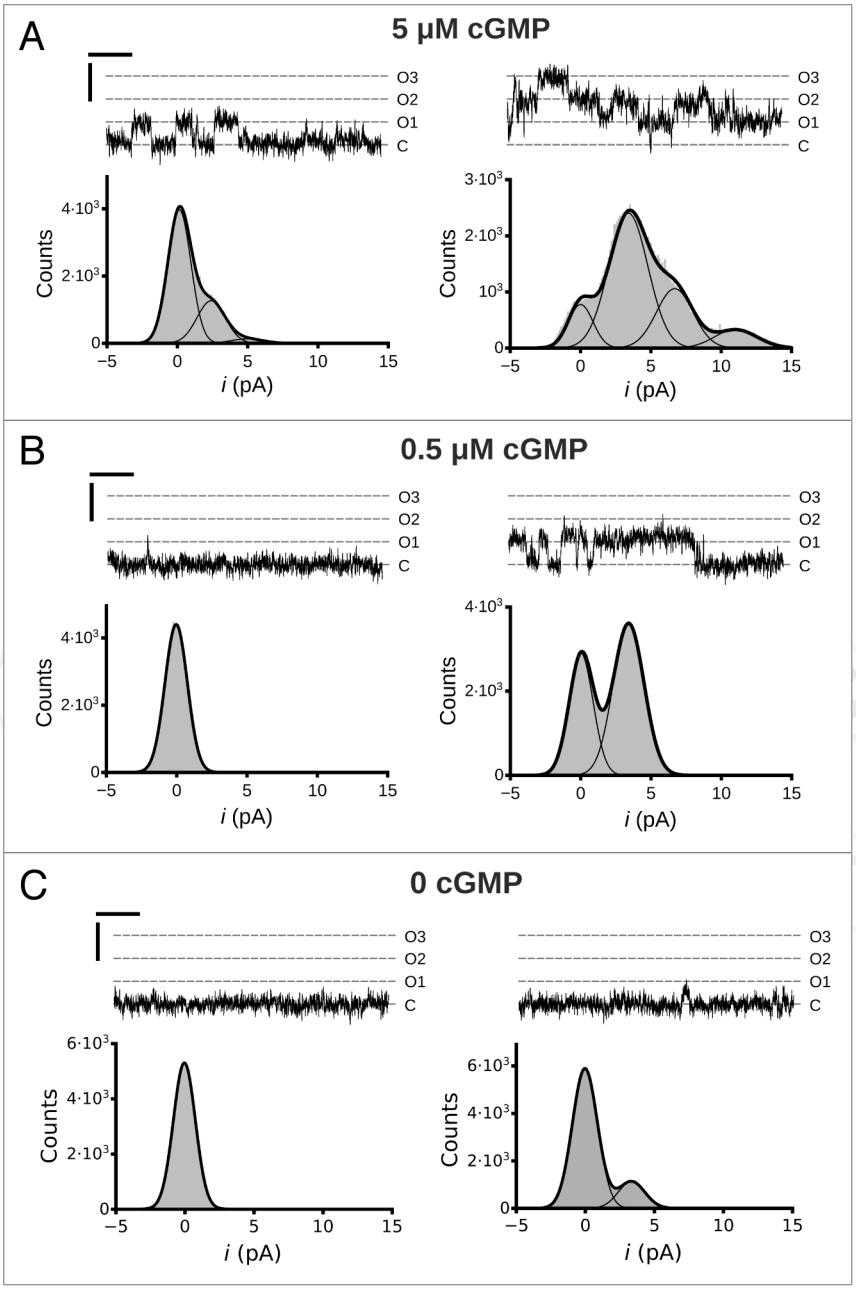

Figure 2. Single channel activity of MMP9 treated CNGA3 homomeric channels. Representative traces from an inside-out patch containing three CNG channels at cGMP concentrations of 5 µM (A), 0.5 µM (B) and 0 (C) at 5 min (t_5, left column) and ~30 min (t_{30}, right column) following excision. Currents were elicited at a membrane potential of +80 mV. *C*, closed channel mean current level; *O*, current level(s) for open channel(s). Current-amplitude histograms were amassed from 4–6 sec of recording and fit by either a single Gaussian function or the sum of multiple Gaussian functions (as indicated). The open probabilities (P_O) for the different cGMP concentrations are as follows: (A) 5 µM cGMP, $P_{O,t5} = 0.11$, $P_{O,t30} = 0.43$; (B) 0.5 µM cGMP, $P_{O,t5} < 0.01$, $P_{O,t30} = 0.20$ (C) 0 cGMP, $P_{O,t5} < 0.01$, $P_{O,t30} = 0.06$. The best-fit Gaussian curves produced the following unitary current (*i*) amplitude estimates: $i_{t5} = 2.5$ pA; $i_{t30} = 3.4$ pA. Scale bars: 50 msec; 5 pA.

and cAMP efficacy following MMP9 treatment. We found that neither disruption of integrin-mediated cell adhesion with the peptide GRGDSP, nor destabilization of the actin cytoskeleton with cytochalasin D, prevented the MMP-associated increase in apparent cGMP affinity (**Fig. 4A** and left) or the increase in cAMP efficacy (**Fig. 4A** and right). These results indicate that the MMP-associated changes in CNG channel ligand sensitivity do not depend on two common, indirect pathways for MMP action.

To examine the specificity of the channel gating effects produced by MMP9 treatment, we determined the effects of other extracellular proteases on CNG channel gating. The two largest families of extracellular proteases are metalloproteinases and serine proteases.[44] We compared the gating effects of MMP9 with those produced by a closely related gelatinase/metalloproteinase (MMP2), a dissimilar metalloproteinase (collagenase), and an extracellular serine protease (trypsin). Within 40 min of exposure, MMP2 produced an increase in cGMP apparent affinity that was indistinguishable from the effect produced by MMP9 (**Fig. 4B**). Treatment with MMP2 also produced a similar increase in cAMP efficacy (data not shown). In contrast, application of neither trypsin nor collagenase produced gating effects similar to those produced by application of MMP9. These results suggest a common or overlapping mechanism for gelatinase modification of CNG channel gating that is not a general feature of extracellular protease activity.

MMP directed gating effects are influenced by channel state. To gain additional mechanistic insight into how MMP treatment alters gating, we determined whether the rate of the gating modification by MMP is sensitive to channel activation state. We compared the time-dependent changes in channel gating properties, measured at 10 min intervals, while maintaining the channels under different cGMP concentrations during the intervening sequences between measurements. For studies described above, the patch was maintained in cyclic nucleotide-free control solution between dose-response measurements such that channels were predominantly in the closed state. When channels were maintained in the open state by the continuous application of a saturating concentration of cGMP (1 mM), the MMP-dependent gating effects were significantly diminished compared with channels maintained in the closed state (zero cGMP) (**Fig. 5A and B**). Interestingly, when channels were maintained in a sub-saturating cGMP concentration—scaled to slightly less than the $K_{1/2}$ cGMP—the gating changes developed more rapidly than when held in either the open or closed states (**Fig. 5A and B**). We observed a similar enhancement in the presence of a saturating concentration of the partial agonist cAMP (data

not shown). This implies that the activation state of the channel, rather than cyclic nucleotide binding-site occupancy, is the key determinant for the observed state dependence.

Gating modifications are associated with proteolytic modification of core channel subunits. To gain additional mechanistic insight on how MMPs alter gating, we examined the kinetic properties of the gating changes for CNGA3 channels. MMP-modified channels exhibit an increased apparent affinity for cGMP; therefore, we used the current in sub-saturating cGMP (2 μM) during the onset and early phase of the gating changes as a reporter for the modifications. We observed a progressive increase in the sub-saturating current of the form of an enzyme-progress curve, with an early nonlinear component followed by a protracted linear phase (**Fig. 6A**). For enzyme kinetic analysis, the slope of the linear phase is a measure of enzyme velocity, which increases to saturation (V_{MAX}) with an increasing substrate concentration. To examine, the kinetic relationship between the CNG channel expression density and the rate of the gating changes, we plotted the change in the sub-saturating current density vs. the patch channel density (estimated from the maximal current and membrane patch area) and fit these with the Michaelis-Menten equation (**Fig. 6B and C**). The data were well fit by the Michaelis-Menten equation [V_{MAX} = 0.5 ± 0.03 pA•(μm^2•sec)$^{-1}$; K_M = 177 ± 26 channels], consistent with direct proteolytic action of MMPs on CNG channels. Because the channels are restricted to the patch surface, the availability of substrate (i.e., channel subunits) at high channel densities is expected to exceed the availability of MMP9 to the membrane patch. This is compatible with a saturable relationship between CNG channel density and the rate of channel modification.

To further test the possibility that the MMP-mediated gating effects may be due to direct proteolytic modification of channel subunits, we exposed intact oocytes expressing CNGA3 tagged with the 3xFLAG epitope at the N-terminus (FLAG-CNGA3), to a solution containing MMP2 and -9. Oocytes were exposed to MMPs for 1 h followed by immunoblot analysis as described in *Materials and Methods*. Full-length subunits were detected at approximately 75, 82 and 85 kDa, while the most prominent putative subunit proteolytic fragments were detected at approximately 38 and 50 kDa. With application of MMP2/9, we observed a decrease in the abundance of a ~75 kDa form of the CNGA3 subunit. This band represents the mostly non-glycosylated form of CNGA3,[45] which is known to form functional channels.[46] MMP2/9 application was associated with an increase in an apparent ~50 kDa fragment and a decrease in an apparent ~38 kDa band (**Fig. 7**). These results were observed also in the presence of an EDTA-free protease inhibitor cocktail (cOmplete Mini EDTA-free, Roche) (data not shown). This inhibitor cocktail is designed to inhibit most major classes of proteolytic enzymes with minimal inhibition of metalloproteinases. The predominant immunoreactive bands were not observed in uninjected oocytes or in the absence of primary antibody (data not shown). These data support the idea that extracellular application of MMP2 and -9 promotes proteolysis of CNGA3 subunits.

MMP9 increases the ligand sensitivity of recombinant and native heteromeric CNG channels. Since native cone

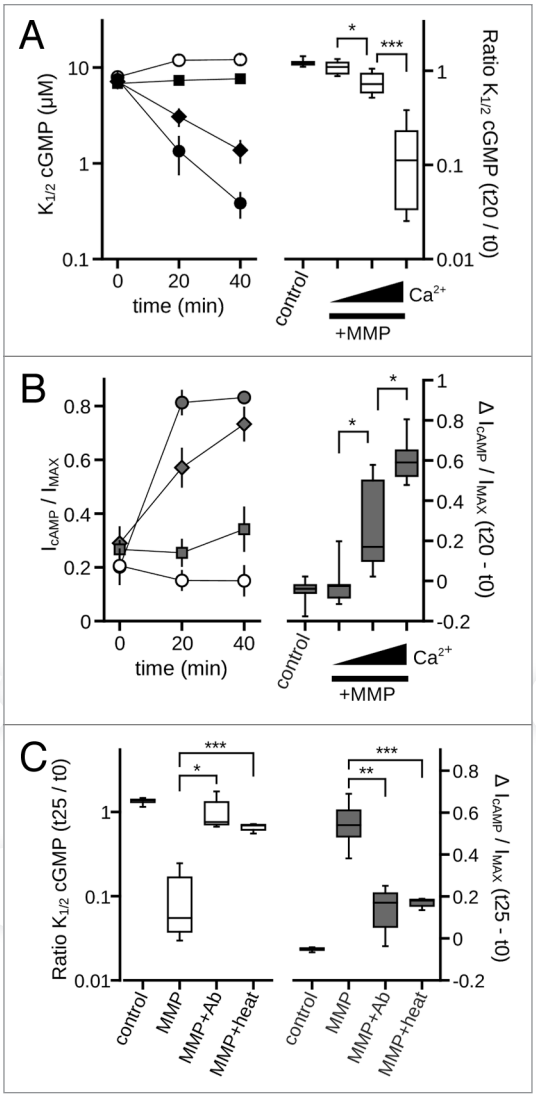

Figure 3. Inhibition of catalytic activity attenuates MMP9 induced gating effects. (A) (Left) Time course of the change in $K_{1/2}$ cGMP for control (open circles) and MMP-treated patches with varying levels of calcium chelation as indicated in Materials and Methods (calcium free, squares; standard calcium, diamonds; elevated calcium, circles). (Right) Box plots summarize the $K_{1/2,cGMP}$ change as ratios between the initial (t_0) and 20 min (t_{20}) values (boxes represent 25th to 75th percentiles, lines represent the median, and whiskers represent the 5th to 95th percentiles). Increasing concentration of free calcium significantly enhanced the $K_{1/2,cGMP}$ change [single-factor ANOVA (n = 6), $p < 0.0001$, Holm's t-test, *$p < 0.05$, ***$p < 0.01$]. (B) (Left) Time course of the change in cAMP efficacy for control (open circles) and MMP-treated patches with varying levels of free calcium [filled symbols, as in (A)]. (Right) Box plots summarizing the change in cAMP efficacy from the initial value at 20 min post excision. Increasing the concentration of free calcium significantly increased cAMP efficacy ($p < 0.0001$, single-factor ANOVA, n = 6; *$p < 0.05$, Holm's t-test). (C) Box plots summarizing the change in $K_{1/2,cGMP}$ (Left) and the change in cAMP efficacy (Right) approximately 25 min post excision. Coapplication of a function-blocking antibody with MMP9 (MMP + Ab) or heat denaturation of MMP9 (MMP + heat) significantly reduced the effect of MMP9 on gating ($p < 0.0001$, single-factor ANOVA, n = 3–6; *$p < 0.05$, **$p < 0.01$, ***$p < 0.001$, Holm's t-test).

©2011 Landes Bioscience. Do not distribute.

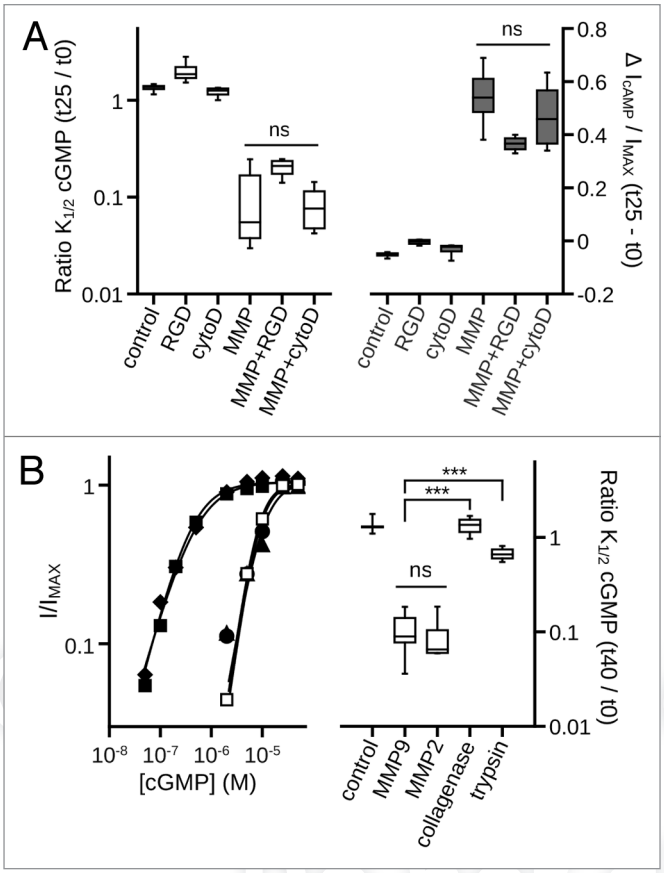

Figure 4. Disruption of the actin cytoskeleton or of integrin mediated cell adhesion does not prevent MMP9 induced gating effects. (A) Box plots summarizing the change in $K_{1/2,cGMP}$ (Left) and the change in cAMP efficacy (Right) approximately 25 min post excision. Neither the integrin adhesion peptide antagonist GRGDSP (MMP + RGD), nor disruption of the actin cytoskeleton by cytochalasin D, significantly altered the change in $K_{1/2,cGMP}$ or in cAMP efficacy induced by MMP9 ($p > 0.1$, single-factor ANOVA analysis performed among MMP9-treatment conditions, n = 4–7). (B) Representative dose-response curves for activation of control (open squares), and protease treated (filled symbols) A3 channels by cGMP at t_{40} (Left). Currents were normalized to the maximum t_{40} cGMP current. Parameters of best fit Hill curves for each condition shown are as follows: control, $K_{1/2}$ = 8.0 μM, n_H = 2.3; MMP9 (filled squares), $K_{1/2}$ = 0.4 μM, n_H = 1.3; MMP2 (filled diamonds), $K_{1/2}$ = 0.5 μM, n_H = 1.2; trypsin (filled triangles), $K_{1/2}$ = 10.0 μM, n_H = 1.9; collagenase (filled circles), $K_{1/2}$ = 8.6 μM, n_H = 2.3. Box plots summarizing the change in $K_{1/2,cGMP}$ approximately 40 min post excision (Right). MMP2 (10 nM) produced gating effects indistinguishable from MMP9 (10 nM). Application of either trypsin (10 nM) or collagenase (100 nM) failed to produce similar gating effects.

photoreceptor CNG channels are heterotetramers containing CNGB3 subunits, we examined the effects of MMP9 on patches excised from oocytes expressing both CNGA3 and CNGB3. Similar to the effects seen with homomeric channels, MMP9 exposure decreased the $K_{1/2}$ cGMP of heteromeric CNGA3 + CNGB3 channels compared with time-matched controls ($K_{1/2,GMP}$: $MMP9_{80\ min}$ = 2.2 μM ± 0.6; $control_{80\ min}$ = 16.4 μM ± 1.2; $p < 0.001$, Aspen-Welch t-test; n = 4–6) (**Fig. 8A and B**) and decreased the maximum current in saturating cGMP. The concentration of cGMP underlying the dark current in photoreceptors is thought to be about 2 to 4 μM.[47] To examine the current produced by heteromeric CNGA3 + CNGB3 channels exposed to an approximately physiological concentration of cGMP, we plotted the 2 μM cGMP-induced current for MMP treated and untreated channels (**Fig. 8C and D**). The increased apparent affinity for cGMP results in a dramatic increase in the 2 μM current ($I_{2\ \mu M}/I_{MAX}$: $MMP9_{80\ min}$ = 0.51 ± 0.05; $control_{80\ min}$ = 0.03 ± 0.006; $p < 0.01$, Aspen-Welch t-test; n = 4–6). These gating changes also were accompanied by increased cAMP efficacy (I_{cAMP}/I_{MAX}: $MMP9_{80\ min}$ = 0.84 ± 0.01; $control_{60\ min}$ = 0.31 ± 0.03; $p < 0.001$, Student's t-test; n = 4–6). The results indicate that heteromeric channels having the native composition of cone photoreceptor CNG channels are susceptible to MMP-mediated gating modifications.

MMP application also caused a slowing of deactivation and an increase in persistent current after removal of cGMP (**Fig. 8E**); the mean steady-state current in the absence of cyclic nucleotides increased from 0.02 ± 0.01 to 0.08 ± 0.03 relative to I_{MAX} for MMP-treated patches within 40 min of excision. The increased persistent current after MMP9 was inhibited by tetracaine, a known CNG channel blocker (data not shown), ruling out patch deterioration as a possible cause. Channel deactivation at t_0 for MMP treated patches was indistinguishable from control patches (data not shown). Furthermore, we did not observe a change in the persistent current within 40 min of excision for control patches (**Fig. 8E** and right). The increase in current in the absence of cyclic nucleotides is consistent with increased spontaneous channel opening, which suggests that MMPs modify the intrinsic, ligand-independent gating properties of the channels.

Native rod photoreceptor CNG channels are heterotetramers containing CNGA1 and CNGB1 subunits.[48-51] To determine if MMP9 alters the ligand sensitivity of rod CNG channels, we examined the effects of MMP9 on cells expressing CNGA1 alone, or CNGA1 coexpressed with CNGB1. Similar to the effects seen with cone CNG channels, MMP9 treatment increased the apparent cGMP affinity for both homomeric channels ($K_{1/2,GMP}$: $MMP9_{40\ min}$ = 2.0 μM ± 0.6; $control_{40\ min}$ = 34.6 μM ± 8.2; $p < 0.01$, Aspen-Welch t-test; n = 3) (**Fig. 9A and B**) and heteromeric channels ($K_{1/2,GMP}$: $MMP9_{40\ min}$ = 4.5 μM ± 0.5; $control_{40\ min}$ = 46.4 μM ± 4.7; $p < 0.001$, Student's t-test; n = 3) (**Fig. 9C and D**) relative to time-matched controls. These changes were also accompanied by an increase in cAMP efficacy for both homomeric channels (A1, I_{cAMP}/I_{MAX}: $MMP9_{30\ min}$ = 0.69 ± 0.03; $control_{30\ min}$ = 0.02 ± 0.01; $p < 0.001$, Student's t-test; n = 3) and heteromeric channels (A1B1, I_{cAMP}/I_{MAX}: $MMP9_{30\ min}$ = 0.74 ± 0.01; $control_{30\ min}$ = 0.08 ± 0.03; $p < 0.001$, Student's t-test; n = 3). For control patches, the previously characterized run-up (increase) in ligand sensitivity that is associated with tyrosine dephosphorylation was observed.[52] Together, these data indicate that sensitivity to MMP9 is a general feature of both cone and rod CNG channels.

Next, we investigated the relative contributions of the different subunit types to the MMP9 mediated gating effects. As described above, homomeric channels formed by rod or cone α subunits (A1 or A3) were sufficient for gating changes. Potential MMP effects on CNGB1 or CNGB3 subunits cannot be directly tested since they fail to form functional homomeric channels in

©2012 Landes Bioscience. Do not distribute

heterologous expression systems.[49,53] The subunit stoichiometries of heteromeric CNG channels are thought to be 3:1 CNGA1 to CNGB1 for rod channels[54-56] and 2:2 CNGA3 to CNGB3 for cone channels.[57] If the gating changes produced by MMPs were primarily due to modification of the α-subunits, we would expect to see a reduced MMP effect for the heteromeric channel configurations. To better quantify the MMP9-associated changes in gating, we fit dose-response data for cone and rod channels with a simple allosteric model, as described in *Materials and Methods* (**Fig. 10A and B**). For all channel configurations, MMP9 increased the equilibrium constant for the allosteric transition associated with channel opening relative to time-matched controls. However, the MMP-dependent changes in the free-energy difference of the opening transition (ΔΔG) for homomeric rod and cone channels were significantly greater than that of their corresponding heteromeric configurations [$p < 0.001$, 2-factor ANOVA, (channel type) x (subunit heterogeneity); independent effect of subunit heterogeneity; n = 3–7] (**Fig. 10C**). Interestingly, the ΔΔG for the heteromeric cone CNG channel is approximately 1/2 that of its homomeric complement ($\Delta\Delta G_{A3/B3}/\Delta\Delta G_{A3} = 0.49 \pm 0.04$), and the ΔΔG for the heteromeric rod channel is roughly 3/4 that of its homomeric complement ($\Delta\Delta G_{A1/B1}/\Delta\Delta G_{A1} = 0.77 \pm 0.05$). These results suggest that either MMP9 does not modify CNGB1 or CNGB3 subunits, or that MMP modification of the B subunits does not appreciably alter channel gating.

Since heterologously expressed CNG channels exhibited dramatic changes in ligand sensitivity with MMP9, we tested whether extracellular MMP9 exposure also alters the gating properties of native photoreceptor CNG channels. We applied MMP9 to native rod CNG channels in inside-out patches excised from Xenopus rod outer segments. The initial $K_{1/2}$ cGMP for the native CNG channels was 23.5 ± 2.1 μM, similar to previous studies of other amphibian rod photoreceptor CNG channels.[58] Consistent with the effects on heterologously-expressed channels, MMP9 increased the apparent affinity for cGMP (**Fig. 11A and C**) and the efficacy of cAMP (**Fig. 11B and C**) relative to time-matched controls. We also observed a decrease in the maximal current elicited by saturating cGMP. These results show that MMPs can enhance native CNG channel sensitivity to cyclic nucleotides.

We have previously noted that MMP9 levels are elevated in the hippocampus of aged animals (unpublished observations). The current study suggests that retinal MMPs could have important regulatory consequences for CNG channels. Therefore, we examined CNGA1 proteolysis and MMP9 levels in retinal tissue from young and aged mice. A pronounced increase in apparent CNGA1 proteolytic fragments was observed with aged retinas, detected using an antibody directed against a CNGA1 C-terminal domain epitope, in the absence of exogenously applied MMP (**Fig. 11D**). We next examined endogenous MMP9 levels in retinas of young and aged mice. MMP9 typically exists as an approximately 90–105 kDa zymogen or one of several lower molecular weight active forms following proteolytic processing.[8,59,60] Retinal tissue from aged animals had dramatically higher levels of the approximately 65 kDa active form of MMP9 (**Fig. 11E**). Upper molecular weight forms were observed with longer film-exposure times (data not shown).

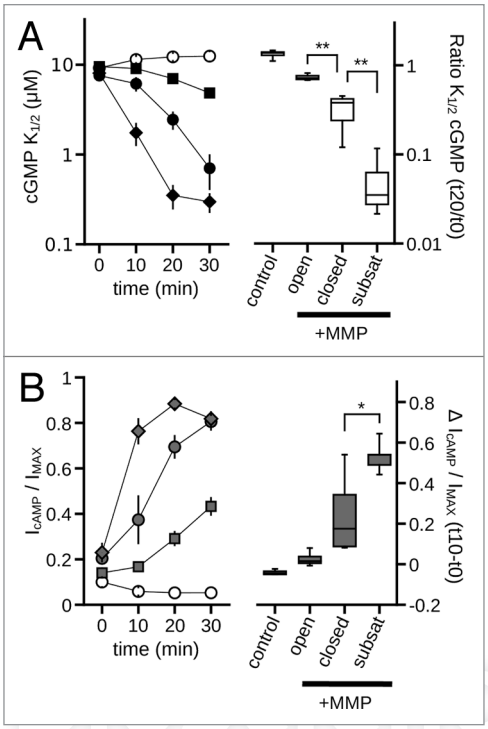

Figure 5. MMP9 directed gating effects are influenced by channel state. (A) (Left) Time course of the change in $K_{1/2,cGMP}$ for control (open circles) and MMP-treated patches exposed to varying concentrations of cGMP to influence channel state: open (1 mM cGMP), squares; closed (zero cGMP), circles; sub-saturating cGMP (graded, 0.2 to 2 μM), diamonds. (Right) Box plots summarize the $K_{1/2,cGMP}$ change as ratios between the initial (t_0) and 20 min (t_{20}) values. Exposure to cGMP significantly impacted the MMP9 induced $K_{1/2,cGMP}$ change ($p < 0.0001$, single-factor ANOVA, n = 4–5). Individual comparisons demonstrate that maintaining channels in the open state significantly attenuated the $K_{1/2,cGMP}$ change, whereas exposure to sub-saturating cGMP significantly enhanced the $K_{1/2}$ change compared with the closed state (**$p < 0.01$, Holm's t-test, n = 4–5). (B) (Left) Time course of the change in cAMP efficacy for control (open circles) and MMP9-treated patches exposed to varying levels of cGMP (filled symbols, as in (A)). (Right) Box plots summarize the change in cAMP efficacy at 10 min post excision compared with the initial value. Exposure to cGMP significantly impacted the change in cAMP efficacy ($p < 0.01$, single-factor ANOVA, n = 4–5). The efficacy of cAMP was significantly elevated after 10 min for patches exposed to sub-saturating cGMP (*$p < 0.05$, Holm's t-test, n = 4–5).

In order to determine if MMP exposure can lead to increased CNGA1 proteolysis within the retina, whole mouse retinas were exposed to exogenous MMPs as described in *Materials and Methods*. In aged animals, prominent bands were consistently observed at approximately 50 kDa, 28 kDa and 23 kDa (**Fig. 11F** and left). Although less abundant, these bands were also present in retinas from young animals and in old retinas not exposed to exogenous MMPs. The ~28 kDa fragment in particular was increased in the urea-soluble fraction from both young and aged retinal tissue with exogenous MMP application (**Fig. 11F** and right). Together these data suggest that endogenous MMP-mediated proteolytic processing, along with other potential proteolytic events, occurs with rod photoreceptor CNG channels, and that this processing may be augmented in the aged retina.

©2012 Landes Bioscience. Do not distribute.

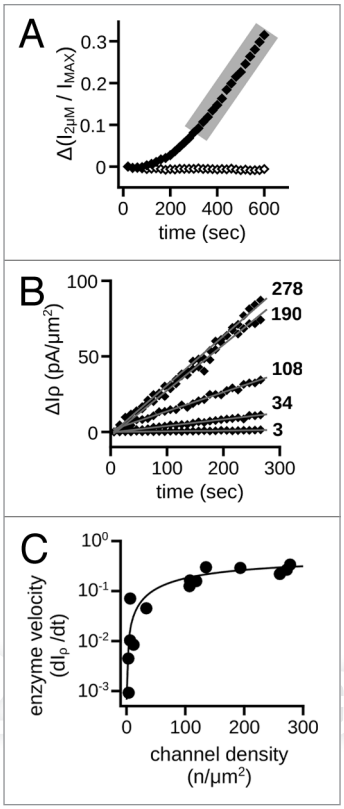

Figure 6. Rate of ligand-sensitivity change is sensitive to channel density. (A) Representative time course demonstrating the change of current in the presence of a sub-saturating concentration of cGMP (2 μM) for control (open diamonds) and 10 nM MMP9 treated (filled diamonds) patches immediately following excision. The 2 μM current was normalized to the saturating cGMP current (I_{MAX}). Shaded area highlights the linear phase of the gating change. (B) Scatter plot of the linear phases of representative time courses with varying channel densities for patches treated with MMP9. Data expressed as the change in the 2 μM current density (ΔI_ρ). Approximate channel densities for each time course (listed on right) were calculated with membrane patch area estimates.[84] Gray lines represent linear fits, with the following best-fit slopes: (in ascending order, pA•(μm²•sec)$^{-1}$) 0.0046, 0.043, 0.12, 0.30 and 0.33. (C) Best-fit slopes were plotted against the estimated channel densities for MMP9 treated patches and fit with the Michaelis-Menten equation with the following best-fit parameters and 95% confidence intervals: K_M = 177 ± 26 channels; V_{MAX} = 0.5 ± 0.03 pA•(μm²•sec)$^{-1}$.

Discussion

We experimentally addressed several possible mechanisms that could explain the MMP-mediated change in CNG channel gating. One possibility is that direct binding of MMP9, or of MMP9-generated proteolytic fragments, to the channel stabilizes the open state relative to the closed state. In other systems, MMPs have been shown to promote shedding of cell adhesion molecules, allowing the liberated fragment to activate cell surface receptors. For instance, MMP9 promotes shedding of ICAM5,[5,61] producing an ectodomain capable of activating integrin signaling cascades.[43] At least two observations preclude these potential mechanisms for the observed gating effects. First, inhibition of MMP catalytic activity interferes with the MMP-mediated gating changes. This suggests that the gating effects are not solely due to a binding interaction between MMPs and the CNG channels. Second, the gating effects are delayed by maintaining the channels in the open state. This delay would seem unlikely if binding of MMP or of MMP-generated fragments served to stabilize the open state, as in this scenario we would expect that maintaining the channels in the open state (saturating cGMP) would accelerate rather than slow the rate of gating changes produced by MMP9.

Another possible explanation for how MMPs increase the ligand sensitivity of CNG channels is via activation of MMP-sensitive signaling cascades (e.g., cytoskeletal-associated or adhesion-sensitive kinases), which in turn could alter gating. Our observations do not support these possible scenarios. First, two common downstream targets of MMP-directed proteolysis are integrin signaling and cytoskeletal remodeling; neither interference with integrin mediated cell adhesion using an RGD peptide, nor destabilization of filamentous actin with cytochalasin D, significantly altered the effect of MMPs on CNG channel gating. Second, the state-dependence of the gating change is largely inconsistent with a downstream effector allosterically stabilizing the open state: maintaining the channels in the open state *delayed* rather than promoted the increase in ligand sensitivity. In contrast, a phosphorylation/dephosphorylation event that alters channel gating typically occurs most efficiently in the channel state stabilized by the modification.[62] This makes it unlikely that the MMP directed gating changes are due solely to the binding of a potentiating downstream effector or phosphorylation/dephosphorylation by a downstream kinase/phosphatase.

Given the evidence described above, we propose instead that MMPs modulate CNG channel function through direct enzymatic processing of the channel. This relationship is supported by observations that the gating changes were dependent on MMP catalytic activity, that the temporal properties of the gating changes are described well by Michaelis-Menten kinetics, and by evidence of increased subunit proteolysis in the presence of exogenously applied MMPs or elevated endogenous levels of retinal MMP9. How might MMP-directed proteolysis increase the ligand sensitivity of CNG channels? The increased ligand sensitivity could result from either an enhancement of the initial ligand-binding step, by altering ligand-specific stabilization of the open state, or via a global effect on the intrinsic gating properties of the channel. The latter mechanism seems more likely for at least three reasons: (1) MMP9 was restricted to extracellular surface of the channel, which is distant from the cyclic nucleotide-binding domain; (2) the MMP-mediated ΔΔG for channel activation by cAMP was similar in magnitude to the ΔΔG for activation by cGMP (data not shown); and (3) MMP exposure increased spontaneous channel openings in the absence of ligand. The magnitude of the MMP effects were larger for homomeric channels compared with heteromeric channels, suggesting the CNGA subunits are key mediators of the MMP associated gating changes. This implies that either CNGB subunits are not modified by MMPs, or that modification of the B subunits does not alter channel gating. The stoichiometries of A to B subunits for heteromeric rod and cone channels are thought to be 3:1 and 2:2,

© 2012 Landes Bioscience

respectively. The reduced change in free energy difference with MMP for heteromeric channels appears to reflect the stoichiometry of A to B subunits for both the rod and cone CNG channels. This disparity between homomeric and heteromeric channels is similar to the change in free energy difference produced by protonation of pH-sensitive residues in rod CNGA1,[63] which are absent in CNGB1. Our results suggest that multiple CNGA subunits can be modified by MMPs, such that successive modifications serve to further enhance ligand sensitivity. Consequently, as modifications progress, there would likely be multiple subpopulations with varying ligand sensitivities based on the number of subunits modified. Such heterogeneous ligand sensitivities could underlie the reduced Hill slope for MMP-treated patches. In light of our current findings, we propose that modification of CNG channels by endogenous MMPs may contribute to differences in the Hill slopes of dose-response relationships previously observed between single-channel patches (n_H = ~3) and macroscopic current recordings (n_H = ~2).[64]

Maintaining the channels in saturating cGMP delayed the MMP associated gating effects. This suggests that key structural elements of the channel are unavailable for modification while the channels are in the open state, but available while in the closed state. Paradoxically, the gating effects were enhanced by maintaining the channels in a sub-saturating concentration of cGMP. One possible explanation is that channels may be most sensitive to MMP modification while in a putative closed-intermediate state. This could entail that ligand-bound, *activated* or *primed* subunits in closed channels are particularly susceptible to the MMP-directed effects. Another possibility is that the gating change is a compound process, requiring entry into both closed and open states—a condition that would be enhanced in sub-saturating ligand conditions. Further work is necessary to characterize the accelerated gating effects at lower open probabilities.

Application of exogenous MMPs to isolated retinas increased putative CNGA1 proteolytic products. Low levels of similarly-sized fragments were present in non-MMP treated retinas, suggesting that similar proteolytic events are occurring to native CNGA1 subunits because of endogenous proteases. The presence of multiple CNGA1 proteolytic products may be due to multiple cleavage events by the exogenous MMPs, and/or subsequent processing by endogenous proteases after a single MMP cleavage. Additionally, increased endogenous CNGA1 proteolysis was evident in the retinas of aged mice compared with young mice. Interestingly, the enhanced age-related proteolysis is concomitant with increased levels of an active MMP9 isoform. Although future studies are needed to characterize the age related increase in MMP9 expression and putative CNGA1 proteolysis, in light of the work presented here, we speculate that the enhancement of CNGA1 proteolysis is due to increased retinal MMP activity. Inferring the putative MMP-cleavage sites from the apparent size of channel fragments is problematic due to the known anomalous migration of CNG channel subunits with SDS-PAGE. Ongoing studies are directed at identification of specific proteolytic site(s).

Proteolytic modification of ion channels can serve to decrease or increase expression or activity of ion channels, thereby altering

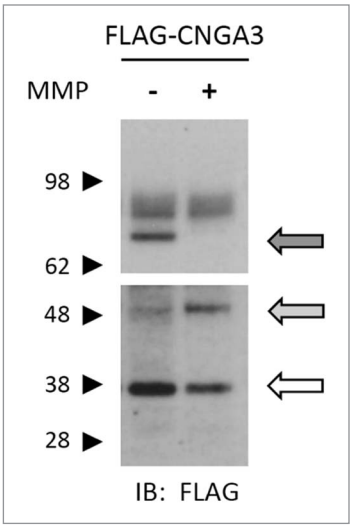

Figure 7. Application of MMP2 and -9 promotes proteolysis of CNGA3 subunits. Western blot analysis is shown for protein lysates from oocytes expressing FLAG-CNGA3 subunits. Intact oocytes were treated with MMP2 and -9 (100 μg/mL total) for 1 h; protein immunoreactivity was assessed using anti-FLAG antibody. MMP9/2 exposure caused a decrease in the bands associated with the full-length CNGA3 subunit (dark arrow) and a corresponding increase in a lower molecular weight form (gray arrow). The blot image was divided into two sections; the upper section had a shorter film-exposure time than the lower section.

cell and tissue function. For example, MMP-mediated proteolysis of NMDA receptors has been shown to decrease channel activity and/or functional cell-surface expression, thereby contributing to activity-dependent changes in neuronal connectivity within the CNS.[34,35] Proteolytic modification of ENaCs governs channel cell-surface expression and gating properties, influencing transepithelial Na^+ transport and ultimately sodium handling within the kidney.[65,66] Along these lines, there are several features of the MMP effects on CNG channels—and what is known about MMPs in the retina—making it plausible that MMPs participate in modifying photoreceptor sensitivity. First, several MMP family members (gelatinases included) are known to be abundant in the retina and present specifically within the interphotoreceptor matrix in proximity to photoreceptor outer segments.[16,17,67] Second, retinal MMP expression appears to be sensitive to ambient light levels, where the onset of normal room-level lighting is sufficient to increase retinal MMP levels.[22] This observation led the authors to speculate on a potential role of MMPs in light adaptation.[22] Third, photoreceptor CNG channels typically exist under conditions of low open probability, where they are most sensitive to the MMP-mediated changes described here (see **Fig. 5**). Finally, the turnover of retinal CNG channels is thought to occur relatively rapidly, with a channel half-life likely less than 12 h.[68] Such rapid turnover rates could allow irreversible modifications—such as channel proteolysis—to participate in circadian regulation of ligand sensitivity.[69] Interestingly, we have observed MMP-dependent decreases in maximum current during extended time courses; thus, MMPs may contribute to channel turnover after prolonged MMP exposure.

©2012 Landes Bioscience. Do not distribute

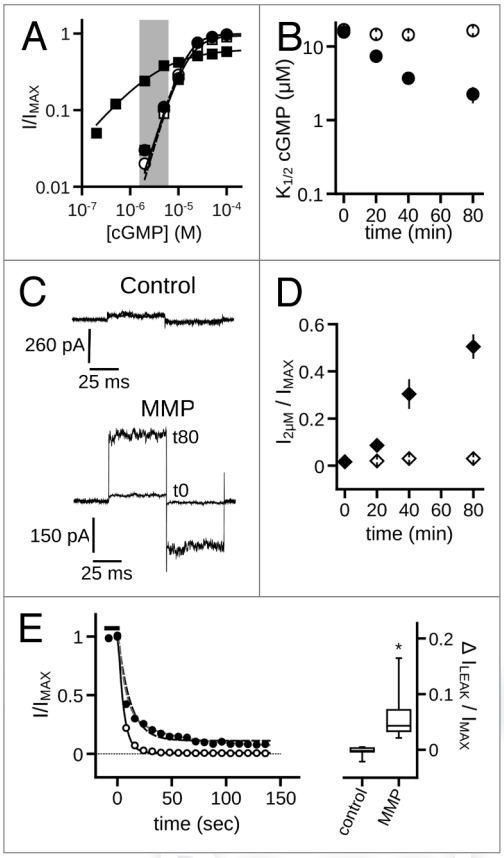

Figure 8. MMP9 increases the ligand sensitivity of heteromeric CNGA3 + CNGB3 channels. (A) Representative dose-response curves for activation of control (open symbols) and MMP9 treated (closed symbols) A3+B3 channels by cGMP at t_0 (circles) and t_{80} (squares). Currents were normalized to the maximum t_0 cGMP current. Shaded area represents approximate physiological cGMP concentration in photoreceptors in the dark.[47] Although prolonged MMP exposure decreases the maximum current in the presence of cGMP (I_{MAX}), channel activation by an approximately physiological concentrations of cGMP is enhanced for MMP-treated patches. Parameters of best fit Hill curves (t_0, hashed line, t_{80}; solid line) for each condition shown are as follows: control, $K_{1/2,t0}$ = 15.7 μM, n_H = 2.1, I_{MAX} = 1.0; $K_{1/2,t80}$ = 16.5 μM, n_H = 1.9, I_{MAX} = 0.94; MMP9, $K_{1/2,t0}$ = 15.2 μM, n_H = 2.2, I_{MAX} = 1.0; $K_{1/2,t80}$ = 3.6 μM, n_H = 0.8, I_{MAX} = 0.75. (B) Time course for the change in cGMP apparent affinity for control (open circles) and MMP9-treated (filled circles) patches following excision. (C) Representative current traces after activation by a sub-saturating concentration of cGMP (2 μM) for control (top) and MMP9-treated (bottom) patches immediately (t_0) and 80 min (t_{80}) following excision. (D) Time course of the 2 μM current for control (open diamonds) and MMP9 treated (filled diamonds) patches following excision. Current normalized to maximal cGMP current (I_{MAX}). (E) (left) Representative time course for current deactivation following removal of a saturating concentration of cGMP (1 mM; black bar) for an MMP treated patch within 5 min (open circles) and approximately 40 min following excision (t_{40}; filled circles). Both groups were normalized to their maximum cGMP current and fit with a single exponential-decay function (black lines) with the following best-fit time constants: τ_{t5} = 5.1 sec; τ_{t4o} = 11.2 sec. The use of a double-exponential function produced a significantly better fit than the single exponential for the t_{40} group (gray line; $p < 0.001$, extra sum-of-squares *F*-test) with the following decay constants: τ_{fast} = 6.2 sec; τ_{slow} = 48.5 sec. Box plots summarizing the change in the persistent current (no cNMP) within 40 min of excision for MMP-treated and control patches (right). Persistent currents were normalized to the maximum cGMP elicited current for each time point. Treatment with MMP9 produced an increase in the persistent current (*$p < 0.05$, Student's t-test, n = 6).

It is likely that in vivo regulation of MMPs is both dynamic and subtle and that physiological alterations in MMP levels could provide a fine tuning of CNG channel ligand sensitivity. The most important implication for the MMP-associated gating effects, however, may be related to retinal disease processes associated with abnormal MMP levels. Increased MMP expression has been linked to rod degeneration in the rd1 mouse,[32] macular degeneration in humans,[27,28] and with retinal excitotoxicity.[20,21,33] Photoreceptor loss is often associated with abnormal CNG channel activity.[70] This can arise from loss of phosphodiesterase activity or increased guanylate-cyclase activity, producing a deleterious elevation of basal cGMP levels,[71,72] or from gain-of-function mutations in CNG channels, resulting in enhanced cyclic nucleotide sensitivity.[73] In these cases, photoreceptor degeneration follows disturbances of calcium homeostasis, which has been shown to promote photoreceptor apoptosis.[74] We speculate that elevated MMPs in the IPM may target outer segment CNG channels, increasing channel ligand sensitivity, potentially contributing to photoreceptor cytotoxicity. Future studies will be directed toward exploring the potential effects of retinal MMPs on photoreceptor function, and investigating whether MMP-associated retinal degeneration is linked to a deleterious enhancement in ligand sensitivity of CNG channels.

Materials and Methods

Molecular biology and functional expression. For heterologous expression in *Xenopus laevis* oocytes, the coding sequence for human CNGA3 [75] was engineered to have an N-terminal 3X-FLAG epitope tag and subcloned into pGEMHE as previously described in reference 57. The human CNGB3 clone was isolated from human retinal cDNA and also subcloned into pGEMHE.[76] FLAG-tagged bovine CNGA1 was generated as previously described in reference 57. HA-tagged human CNGB1 was a generous gift of Dr. S.E. Gordon. Oocytes were isolated and microinjected with a fixed amount of mRNA for all constructs (~5 ng). For efficient generation of heteromeric channels, the ratio of CNGA mRNA to CNGB mRNA was 1:2.5.[57] Oocytes were incubated in ND96 (96 mM NaCl, 2 mM KCl, 1.8 mM $CaCl_2$, 1 mM $MgCl_2$ and 5 mM HEPES, pH 7.6, supplemented with 10 μg/ml gentamycin) at a temperature of 17–19°C.

Electrophysiology. One to 7 d after microinjection of mRNA, patch-clamp experiments were performed in the inside-out configuration. Recordings were made at 20–23°C. Voltage control was provided by an Axopatch 200B amplifier (Axon Instruments); macroscopic current data were acquired using Pulse software (HEKA Elektronik) with a sampling frequency of 25 kHz, low-pass filtered at 2 kHz and initial pipette resistances were 0.4–0.8 MΩ. From a holding potential of 0 mV, currents were elicited by voltage steps to +80 mV, then to -80 mV, and back to 0 mV. Single channel recordings were made at 25 kHz sampling rate, were low-pass filtered at 1 kHz and initial pipette resistances were

1.5–1.8 MΩ. Intracellular and extracellular solutions typically contained 130 mM NaCl, 0.2 mM EDTA and 3 mM HEPES (pH 7.2). The Cyclic nucleotides, cAMP (Sigma-Aldrich, A6885) or cGMP (Sigma-Aldrich, G6129), were added to intracellular solutions as indicated. The intracellular solution applied to the face of the patch was changed using an RSC-160 rapid solution changer (Molecular Kinetics, Indianapolis, IN). Stock solutions of active human recombinant MMP9 (Calbiochem, PF024) or MMP2 (Calbiochem, PF023) were diluted to 1 μg/mL with the extracellular (pipette) solution and added to the patch electrode prior to patch-clamp recording. The MMP stock solutions included 10 mM $CaCl_2$. The free-calcium concentration of the working MMP solutions depended on the amount of divalent chelator present. For inhibition of MMPs, we varied the amount of chelator (i.e., EDTA and EGTA) to alter the level of free calcium and potentially other non-specified divalents. Based on the algorithm in the CHELATOR program,[77] the expected free-calcium concentrations at different levels of chelation were as follows: zero chelation, $1e^{-4}$ M; intermediate chelation, $2.8e^{-7}$ M; high chelation, $2.8e^{-9}$ M. For inhibition with function blocking antibody, 1 μg/mL recombinant MMP9 was pre-incubated with 50 μg/mL anti-MMP9 mouse monoclonal antibody (EMD Chemicals, IM09L) for 10 min prior to its addition to the patch electrode.

For comparative protease experiments, collagenase isolated from *Clostridium histolyticum* (Sigma, C2674) was dissolved in extracellular buffer at a concentration of 10 μg/mL. Trypsin-EDTA (Gibco, 25200) was diluted to a final concentration of 1 μg/mL in extracellular buffer. For integrin destabilization experiments, the peptide GRGDSP (Calbiochem, 03-34-0035) was dissolved to a final concentration of 500 μM in the extracellular solution, and was added to the patch electrode prior to the indicated recordings. For F-actin destabilization, oocytes were pretreated with 10 μM cytochalasin D (Sigma, C2618) in ND96 for 2–4 h prior to indicated recordings.

For native rod CNG channel recordings, retinas were dissected from *Xenopus laevis* and placed in a frog Ringer's solution: 111 mM NaCl, 2.5 mM KCl, 1 mM $CaCl_2$, 1.2 mM $MgCl_2$, 10 mM D-glucose, 0.2 mM EDTA and 3 mM HEPES (pH 7.6). Rod outer segments were isolated by gentle mechanical agitation of the retinal tissue and allowed to settle in the recording chamber. Patch-clamp experiments were performed in the inside-out configuration as described above. Initial pipette resistances were 3–6 MΩ.

Data analysis. Currents were leak subtracted using the current traces elicited in the absence of cyclic nucleotides before analysis unless otherwise indicated. For channel activation by cGMP or cAMP, dose-response data were fit with the Hill equation: $I/I_{MAX} = [cNMP]^{nH}/(K_{1/2}{}^{nH} + [cNMP]^{nH})$, where I is the current amplitude, I_{MAX} is the maximum current elicited by saturating concentration of ligand, [cNMP] is the ligand concentration, $K_{1/2}$ is the apparent ligand affinity, and n_H is the Hill slope. Fitting with the Hill equation was accomplished with Octave, an open source data-analysis package (www.octave.org), using a custom fitting routine based on the method of steepest descent.

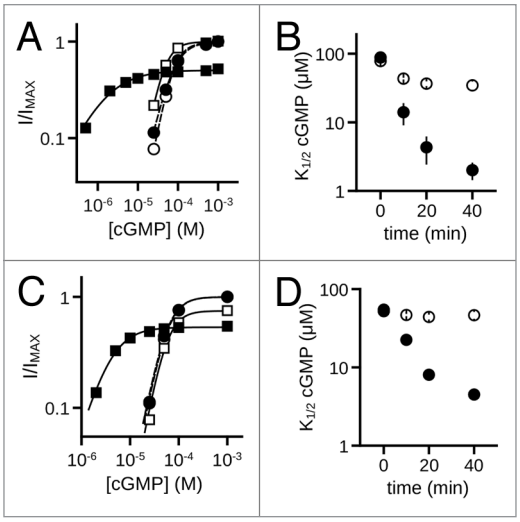

Figure 9. MMP9 increases the ligand sensitivity of rod homomeric CNGA1 and heteromeric CNGA1 + CNGB1 channels. (A) Representative dose-response curves for activation of control (open symbols) and MMP9 treated (closed symbols) A1 channels by cGMP at t_0 (circles) and t_{40} (squares). Currents were normalized to the maximum t_0 cGMP current. Parameters of best fit Hill curves (t_0, hashed line; t_{40}, solid line) for each condition shown are as follows: control, $K_{1/2,t0}$ = 75.9 μM, n_H = 2.2, I_{MAX} = 1.0, $K_{1/2,t40}$ = 43.9 μM, n_H = 2.2, I_{MAX} = 1.0; MMP9 $K_{1/2,t0}$ = 75.3 μM, n_H = 1.8, I_{MAX} = 1.0, $K_{1/2,t40}$ = 1.5 μM, n_H = 0.9, I_{MAX} = 0.50. (B) Time course for the change in cGMP apparent affinity of A1 channels for control (open circles) and MMP9-treated (filled circles) patches following excision. (C) Representative cGMP dose-response curves of control (open symbols) and MMP9 treated (closed symbols) A1+B1 channels at t_0 (circles) and t_{40} (squares). Currents were normalized to the maximum t_0 cGMP current. Parameters of best fit Hill curves (t_0, hashed line; t_{40}, solid line) for each condition shown are as follows: control, $K_{1/2,t0}$ = 59.4 μM, n_H = 2.3, I_{MAX} = 1.0, $K_{1/2,t40}$ = 55.6 μM, n_H = 2.4, I_{MAX} = 0.75; MMP9 $K_{1/2,t0}$ = 57.2 μM, n_H = 2.3, I_{MAX} = 1.0, $K_{1/2,t40}$ = 3.9 μM, n_H = 1.5, I_{MAX} = 0.53. (D) Time course for the change in cGMP apparent affinity of A1+B1 channels for control (open circles) and MMP9-treated (filled circles) patches following excision.

To quantify the MMP-induced gating effects of homomeric and heteromeric channels, we used a simplified linear allosteric model where independent ligand-binding steps are followed by a single allosteric transition from the liganded but closed state to the open state:[78-81]

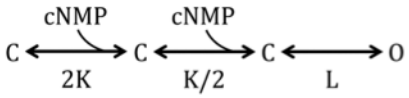

In this kinetic scheme, K is the equilibrium constant for the initial binding of cyclic nucleotide and L is the equilibrium constant of the allosteric conformational transition. The values of L were determined from fits of the allosteric model to the dose-response, where K = 6,000 M^{-1};[45] K was assumed to be unaltered by MMP-mediated channel processing. We limited our analyses to dose-response data collected after maximal gating changes were achieved. Curve fitting with the allosteric model was performed with Octave, using a custom routine based on the method of steepest descent. The free-energy differences were calculated as $\Delta G = -RT \times \ln(L)$; and, $\Delta\Delta G = \Delta G_{MMP} - \Delta G_{control}$.

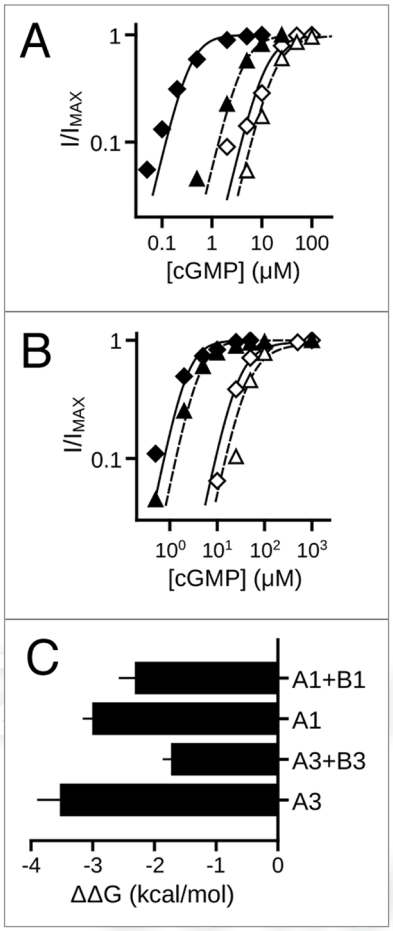

Figure 10. MMP9 induced gating effects are more pronounced for homomeric compared with heteromeric rod and cone CNG channels. (A) Representative dose-response curves for activation of control (open symbols) and MMP9-treated (closed symbols) A3 homomeric (diamonds) and A3+B3 heteromeric (triangles) channels by cGMP, at 80 min post excision. Currents were normalized to the maximum cGMP current. Continuous curves (A3, solid line; A3+B3, hashed line) represent fits with the allosteric model described in Materials and Methods. The best fit equilibrium constants for the allosteric transition (L) for each condition shown are as follows: $A3_{control}$ = 180, $A3_{MMp}$ = 217,000; $A3+B3_{control}$ = 90, $A3+B3_{MMp}$ = 1,700. (B) Representative dose-response curves for activation of control (open symbols) and MMP9-treated (closed symbols) A1 homomeric (diamonds) and A1+B1 heteromeric (triangles) channels by cGMP at 40 min post excision. Currents were normalized to the maximum cGMP current. Continuous curves (A1, solid line; A1+B1, hashed line) represent fits with the allosteric model used in (A). The best fits of L for each condition are as follows: $A1_{control}$ = 40, $A1_{MMP}$ = 5,400; $A1+B1_{control}$ = 20, $A1+B1_{MMP}$ = 1,700. (C) Bar graph showing the change in free energy difference of the allosteric transition associated with the maximal MMP9 induced gating effects for rod and cone homomeric and heteromeric channels; data expressed as mean (±SEM). The change in free energy difference for channel gating was significantly reduced for heteromeric channels compared with homomeric channels [$p < 0.001$, 2-factor ANOVA, (channel type) X (subunit heterogeneity), independent effect of (subunit heterogeneity), n = 3–7].

Protein biochemistry. To examine the proteolytic processing of CNGA3 subunits expressed in Xenopus oocytes, we used immunoblot analysis of proteins from oocytes expressing FLAG-tagged CNGA3. Typically four oocytes per treatment group were carefully stripped of their vitelline membranes and placed together in an Eppendorf tube. Oocytes were exposed either to a mixture of stock MMP9 and MMP2 solutions (100 μg/mL) or an equal volume of MMP vehicle for approximately 1 h at room temperature prior to sample collection. We used an elevated concentration of MMP9 to address the likelihood of increased competitive inhibition from other endogenous MMP substrates (e.g., ECM molecules) present in the whole-oocyte reaction solution. Our results indicate that the gating effects proceed most efficiently in the presence of sub-saturating cGMP (**Fig. 5**). To potentially facilitate proteolysis, 1 μM CPT-cGMP was added to the reaction solution, exposing the channels to a sub-saturating concentration of cGMP during MMP exposure. Oocyte lysates were prepared as previously described in reference 76. Briefly, oocytes were placed in lysis buffer containing: 20 mM HEPES (pH 7.5), 150 mM NaCl, 5 mM EDTA, 0.5% Triton X-100 (Pierce, Surfact-Amps X-100) and protease inhibitors (Roche Applied Science, cOmplete, Mini, EDTA-free Protease Inhibitor Cocktail Tablets). Oocytes were subjected to homogenization and the soluble cell lysate was then separated from yolk and other insoluble material by centrifugation at 20,000 g for 10 min at 4°C. Lysate representing approximately one oocyte per lane was loaded and separated by SDS-PAGE on NuPAGE 4–12% TRIS-acetate gels (Invitrogen, NP0321). Proteins were then transferred to nitrocellulose membrane using the NuPAGE transfer system (Invitrogen). Immunoblots were processed as described previously in reference 57, using an anti-FLAG M2 monoclonal antibody (Sigma-Aldrich, A2220), at a concentration of 1:50,000 in TTBS buffer with 1% nonfat dry milk, followed by chemiluminescent detection (Thermo Scientific, SuperSignal West Dura Substrate). The approximate molecular weights of the FLAG-tagged subunits were estimated using protein standards (SeeBlue Plus2, Invitrogen).

To examine the proteolytic processing of CNGA1 subunits from C57BL6 mouse retina, typically four isolated retinas per treatment group (ages: young, 2–3 mo; old, 12–14 mo), and were subsequently placed in frog Ringer's solution and were exposed either to a mixture of MMP9 and MMP2 solutions (~10 μg/mL) or an equal volume of MMP vehicle for approximately 1 h at room temperature prior to homogenization. Retinal lysates were prepared by homogenization in lysis buffer containing: 20 mM Hepes (pH 7.5), 150 mM NaCl, 5 mM EDTA, 0.5% Triton X-100 (Surfact-Amps X-100, Pierce) and protease inhibitors (cOmplete, Mini, EDTA-free Protease Inhibitor Cocktail Tablets, Roche Applied Science). The detergent soluble cell lysate was then separated from insoluble material by centrifugation at 20,000 g for 10 min at 4°C. The insoluble fraction was resuspended and homogenized in lysis buffer containing 8 M urea and allowed to sit on ice for 2 h, followed by a repeat of centrifugation and separation of the urea soluble fraction. Aliquots of urea soluble fraction for electrophoresis were mixed with SDS loading buffer, heated for 10 min and placed at 4°C overnight. Total protein was normalized between samples using a BSA protein assay (Biorad), prior to loading of SDS-polyacrylamide gels; we loaded 0.6 μg of protein per lane for urea soluble fractions and 1.3 μg of protein per lane for

© 2012 Landes Bioscience. Do not distribute

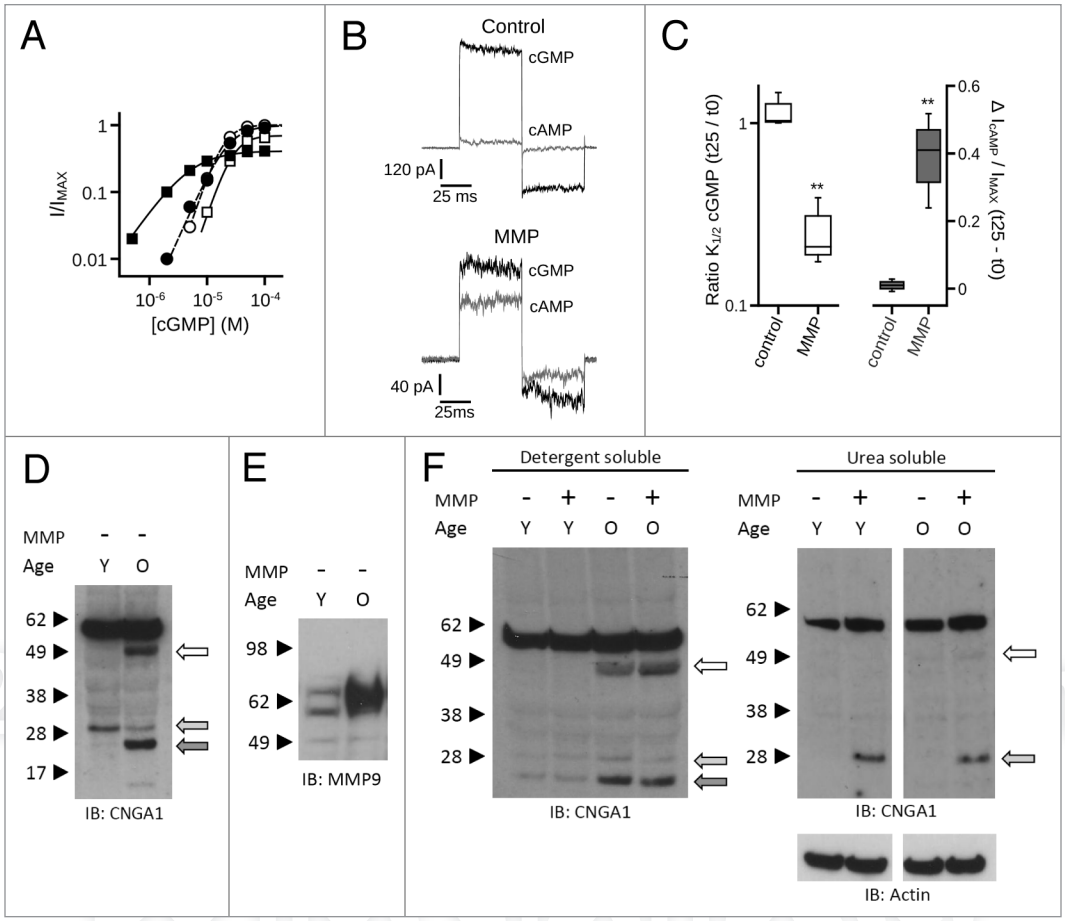

Figure 11. MMPs enhance the ligand sensitivity and apparent proteolysis of native rod photoreceptor CNG channels. (A) MMP9 (10 nM) was applied to the extracellular face of inside-out patches excised from Xenopus rod outer segments. Representative dose-response curves are shown for activation of control (open symbols) and MMP9-treated (closed symbols) rod CNG channels by cGMP at t_0 (circles) and t_{25} (squares). Currents were normalized to the maximum t_0 cGMP current. Parameters of best fit Hill curves (t_0, hashed line; t_{25}, solid line) for each condition shown are as follows: control, $K_{1/2,t0}$ = 19.3 μM, n_H = 2.6, I_{MAX} = 1.0, $K_{1/2,t25}$ = 28.1 μM, n_H = 2.6, I_{MAX} = 0.70; MMP9, $K_{1/2,t0}$ = 22.8 μM, n_H = 2.0, I_{MAX} = 1.0, $K_{1/2,t25}$ = 4.9 μM, n_H = 1.3, I_{MAX} = 0.41. (B) Representative current traces after activation by a saturating concentration of cGMP (1 mM, black line) or cAMP (10 mM, gray line) for control (top) and MMP9-treated (bottom) patches at approximately 25 min following excision. (C) Box plots summarizing the change in $K_{1/2}$ cGMP (Left) and the change in cAMP efficacy (Right) approximately 25 min post excision. Exposure to MMP9 significantly reduced the $K_{1/2}$ cGMP and enhanced the efficacy of cAMP relative to controls (**p < 0.01, Student's t-test, n = 3). (D) Application of MMP2 and -9 promotes proteolysis of native rod CNGA1 subunits in a pattern that mimics existing in vivo proteolytic processing. Western blot analysis is shown of detergent-soluble protein homogenates from mouse retina of "young" (Y, 2–3 mo old) and "old" (O, 12–14 mo old) C57BL6 mice. Intact retinal tissues were treated with MMP2 and -9 (~10 μg/mL total) for 1 h; protein immunoreactivity was assessed using anti-CNGA1 1D1 antibody or anti-MMP9 antibody. Channel subunit proteolytic band patterns differ between young and old mice in the absence of exogenous MMP application. (E) Analysis of MMP9 in these retinas demonstrated elevated levels of a ~65 kDa active form of MMP9 in the old retinas compared with young retinas. (F) MMP9/2 exposure was associated with only a slight increase in the apparent ~50 kDa CNGA1 proteolytic band in the detergent soluble fraction (Left); however, MMP exposure led to a significant increase in the apparent ~30 kDa band in the urea-soluble retinal fraction (Right). This is also a constitutive band (present in tissues not exposed to exogenous MMPs) in both young and old detergent-soluble retinal fractions (F, light gray arrow), and is visible with longer film exposures in the urea-soluble fractions (data not shown).

detergent soluble lysate. Both fractions were separated by SDS-PAGE on NuPAGE 4–12% TRIS-acetate gels (Invitrogen). Proteins were then transferred to nitrocellulose membrane using the NuPAGE transfer system (Invitrogen). Immunoblots were processed as described for oocytes and probed with anti-CNGA1 PMc 1D1 monoclonal antibody (1:1,000),[82] anti-MMP9 rabbit polyclonal antibody (1:1,000) (Abcam, ab38898), or anti-actin (Millipore, MAB1501) followed by HRP-conjugated secondary antibody and chemiluminescent detection (SuperSignal West Dura Substrate, Thermo Scientific). The anti-MMP9 antibody used for these studies recognizes the full-length pro-MMP9 form and multiple active MMP9 fragments. The approximate molecular weights of the channel subunits and fragments were estimated using protein standards (Invitrogen, SeeBlue Plus2).

Statistical analysis. ANOVAs, single-pairwise and multiple-pairwise comparisons were performed with NCSS (www.NCSS.com). Data were tested for normality and equal variance prior to hypothesis testing; data which violated the assumption of equal variance were analyzed with the Aspin-Welch corrected

t-test as indicated. Single pairwise comparisons of normally-distributed and equal-variant (NDEV) data were analyzed with the Student's t-test; multiple pairwise comparisons of NDEV data were analyzed with the Holm-Bonferroni corrected t-test[83] subsequent to statistically significant ANOVA result. A p value less than 0.05 was considered to be statistically significant for all hypothesis tests. All values are reported as the mean ± SEM of *n* experiments (patches) unless otherwise indicated. All graphs were produced with QtiPlot (soft.proindependent.com/qtiplot.html), an open source analysis and graphing program.

Disclosure of Potential Conflicts of Interest

No potential conflicts of interest were disclosed.

Acknowledgments

We are thankful to S.E. Gordon for providing the CNGB1-HA construct, K.W. Yau for sharing the cDNA clone for human CNGA3, W.N. Zagotta for sharing CNGA1 and R. Molday for providing the anti-CNGA1 antibody. We are also grateful for the contributions of D. Sienkiewicz and D. Gabelmann to these studies. This work was supported by grants from the National Eye Institute (EY12836 to M.D.V. and EY19907 to R.L.B.).

References

1. Murphy G, Nagase H. Progress in matrix metalloproteinase research. Mol Aspects Med 2008; 29:290-308; PMID:18619669; http://dx.doi.org/10.1016/j.mam.2008.05.002.
2. Nagy V, Bozdagi O, Matynia A, Balcerzyk M, Okulski P, Dzwonek J, et al. Matrix metalloproteinase-9 is required for hippocampal late-phase long-term potentiation and memory. J Neurosci 2006; 26:1923-34; PMID:16481424; http://dx.doi.org/10.1523/JNEUROSCI.4359-05.2006.
3. Meighan PC, Meighan SE, Davis CJ, Wright JW, Harding JW. Effects of matrix metalloproteinase inhibition on short- and long-term plasticity of schaffer collateral/CA1 synapses. J Neurochem 2007; 102:2085-96; PMID:17587312; http://dx.doi.org/10.1111/j.1471-4159.2007.04682.x.
4. Bilousova TV, Rusakov DA, Ethell DW, Ethell IM. Matrix metalloproteinase-7 disrupts dendritic spines in hippocampal neurons through NMDA receptor activation. J Neurochem 2006; 97:44-56; PMID:16515559; http://dx.doi.org/10.1111/j.1471-4159.2006.03701.x.
5. Tian L, Stefanidakis M, Ning L, Van Lint P, Nyman-Huttunen H, Libert C, et al. Activation of NMDA receptors promotes dendritic spine development through MMP-mediated ICAM-5 cleavage. J Cell Biol 2007; 178:687-700; PMID:17682049; http://dx.doi.org/10.1083/jcb.200612097.
6. Wang XB, Bozdagi O, Nikitczuk JS, Zhai ZW, Zhou Q, Huntley GW. Extracellular proteolysis by matrix metalloproteinase-9 drives dendritic spine enlargement and long-term potentiation coordinately. Proc Natl Acad Sci USA 2008; 105:19520-5; PMID:19047646; http://dx.doi.org/10.1073/pnas.0807248105.
7. Wójtowicz T, Mozrzymas JW. Late phase of long-term potentiation in the mossy fiber-CA3 hippocampal pathway is critically dependent on metalloproteinases activity. Hippocampus 2010; 20:917-21; PMID:20572195.
8. Meighan SE, Meighan PC, Choudhury P, Davis CJ, Olson ML, Zornes PA, et al. Effects of extracellular matrix-degrading proteases matrix metalloproteinases 3 and 9 on spatial learning and synaptic plasticity. J Neurochem 2006; 96:1227-41; PMID:16464240; http://dx.doi.org/10.1111/j.1471-4159.2005.03565.x.
9. Nagy V, Bozdagi O, Huntley GW. The extracellular protease matrix metalloproteinase-9 is activated by inhibitory avoidance learning and required for long-term memory. Learn Mem 2007; 14:655-64; PMID:17909100; http://dx.doi.org/10.1101/lm.678307.
10. Olson ML, Meighan PC, Brown TE, Asay AL, Benoist CC, Harding JW, et al. Hippocampal MMP-3 elevation is associated with passive avoidance conditioning. Regul Pept 2008; 146:19-25; PMID:17698214; http://dx.doi.org/10.1016/j.regpep.2007.07.004.
11. Szklarczyk A, Lapinska J, Rylski M, McKay RDG, Kaczmarek L. Matrix metalloproteinase-9 undergoes expression and activation during dendritic remodeling in adult hippocampus. J Neurosci 2002; 22:920-30; PMID:11826121.
12. Kim HJ, Fillmore HL, Reeves TM, Phillips LL. Elevation of hippocampal MMP-3 expression and activity during trauma-induced synaptogenesis. Exp Neurol 2005; 192:60-72; PMID:15698619; http://dx.doi.org/10.1016/j.expneurol.2004.10.014.
13. Agrawal SM, Lau L, Yong VW. MMPs in the central nervous system: where the good guys go bad. Semin Cell Dev Biol 2008; 19:42-51; PMID:17646116; http://dx.doi.org/10.1016/j.semcdb.2007.06.003.
14. Miller JP, Holcomb J, Al-Ramahi I, de Haro M, Gafni J, Zhang N, et al. Matrix metalloproteinases are modifiers of huntingtin proteolysis and toxicity in Huntington's disease. Neuron 2010; 67:199-212; PMID:20670829; http://dx.doi.org/10.1016/j.neuron.2010.06.021.
15. Yang Y, Hill JW, Rosenberg GA. Chapter 6—multiple roles of metalloproteinases in neurological disorders. Prog Mol Biol Transl Sci 2011; 99:241-63.
16. Plantner JJ, Drew TA. Polarized distribution of metalloproteinases in the bovine interphotoreceptor matrix. Exp Eye Res 1994; 59:577-85; PMID:9492759; http://dx.doi.org/10.1006/exer.1994.1143.
17. Padgett LC, Lui GM, Werb Z, LaVail MM. Matrix metalloproteinase-2 and tissue inhibitor of metalloproteinase-1 in the retinal pigment epithelium and interphotoreceptor matrix: vectorial secretion and regulation. Exp Eye Res 1997; 64:927-38; PMID:9301473; http://dx.doi.org/10.1006/exer.1997.0287.
18. Smine A, Plantner JJ. Membrane type-1 matrix metalloproteinase in human ocular tissues. Curr Eye Res 1997; 16:925-9; PMID:9288454; http://dx.doi.org/10.1076/ceyr.16.9.925.5044.
19. Plantner JJ, Smine A, Quinn TA. Matrix metalloproteinases and metalloproteinase inhibitors in human interphotoreceptor matrix and vitreous. Curr Eye Res 1998; 17:132-40; PMID:9523090; http://dx.doi.org/10.1076/ceyr.17.2.132.5610.
20. Zhang X, Cheng M, Chintala SK. Kainic acid-mediated upregulation of matrix metalloproteinase-9 promotes retinal degeneration. Invest Ophthalmol Vis Sci 2004; 45:2374-83; PMID:15223820; http://dx.doi.org/10.1167/iovs.03-1239.
21. Mali RS, Cheng M, Chintala SK. Intravitreous injection of a membrane depolarization agent causes retinal degeneration via matrix metalloproteinase-9. Invest Ophthalmol Vis Sci 2005; 46:2125-32; PMID:15914633; http://dx.doi.org/10.1167/iovs.04-1376.
22. Papp AM, Nyilas R, Szepesi Z, Lorincz ML, Takács E, Abrahám I, et al. Visible light induces matrix metalloproteinase-9 expression in rat eye. J Neurochem 2007; 103:2224-33; PMID:17854381; http://dx.doi.org/10.1111/j.1471-4159.2007.04917.x.
23. Sivak JM, Fini ME. MMPs in the eye: emerging roles for matrix metalloproteinases in ocular physiology. Prog Retin Eye Res 2002; 21:1-14; PMID:11906808; http://dx.doi.org/10.1016/S1350-9462(01)00015-5.
24. Majka S, McGuire P, Colombo S, Das A. The balance between proteinases and inhibitors in a murine model of proliferative retinopathy. Invest Ophthalmol Vis Sci 2001; 42:210-5; PMID:11133870.
25. Giebel SJ, Menicucci G, McGuire PG, Das A. Matrix metalloproteinases in early diabetic retinopathy and their role in alteration of the blood-retinal barrier. Lab Invest 2005; 85:597-607; PMID:15711567; http://dx.doi.org/10.1038/labinvest.3700251.
26. Kowluru RA. Role of matrix metalloproteinase-9 in the development of diabetic retinopathy and its regulation by H-Ras. Invest Ophthalmol Vis Sci 2010; 51:4320-6; PMID:20220057; http://dx.doi.org/10.1167/iovs.09-4851.
27. Plantner JJ, Jiang C, Smine A. Increase in interphotoreceptor matrix gelatinase A (MMP-2) associated with age-related macular degeneration. Exp Eye Res 1998; 67:637-45; PMID:9990329; http://dx.doi.org/10.1006/exer.1998.0552.
28. Chen YD, Xu X, Xia X, Wu H, Liu K, Zheng Z, et al. MMP9 is involved in glycation end-products induced increase of retinal vascular permeability in rats and the therapeutic effect of minocycline. Curr Eye Res 2008; 33:977-83; PMID:19085380; http://dx.doi.org/10.1080/02713680802450984.
29. Macgregor AM, Eberhart CG, Fraig M, Lu J, Halushka MK. Tissue inhibitor of matrix metalloproteinase-3 levels in the extracellular matrix of lung, kidney and eye increase with age. J Histochem Cytochem 2009; 57:207-13; PMID:18955737; http://dx.doi.org/10.1369/jhc.2008.952531.
30. Liutkeviciene R, Lesauskaite V, Asmoniene V, Zaliūniene D, Jasinskas V. Factors determining age-related macular degeneration: a current view. Medicina (Kaunas) 2010; 46:89-94; PMID:20440081.
31. Mathalone N, Lahat N, Rahat MA, Bahar-Shany K, Oron Y, Geyer O. The involvement of matrix metalloproteinases 2 and 9 in rat retinal ischemia. Graefes Arch Clin Exp Ophthalmol 2007; 245:725-32; PMID:17024442; http://dx.doi.org/10.1007/s00417-006-0362-y.
32. Ahuja S, Ahuja P, Caffé AR, Ekstrom P, Abrahamson M, van Veen T. rd1 mouse retina shows imbalance in cellular distribution and levels of TIMP-1/MMP-9, TIMP-2/MMP-2 and sulfated glycosaminoglycans. Ophthalmic Res 2006; 38:125-36; PMID:16374054; http://dx.doi.org/10.1159/000090533.
33. Chintala SK. The emerging role of proteases in retinal ganglion cell death. Exp Eye Res 2006; 82:5-12; PMID:16185688; http://dx.doi.org/10.1016/j.exer.2005.07.013.
34. Szklarczyk A, Ewaleifoh O, Beique JC, Wang Y, Knorr D, Haughey N, et al. MMP-7 cleaves the NR1 NMDA receptor subunit and modifies NMDA receptor function. FASEB J 2008; 22:3757-67; PMID:18644839; http://dx.doi.org/10.1096/fj.07-101402.
35. Pauly T, Ratliff M, Pietrowski E, Neugebauer R, Schlicksupp A, Kirsch J, et al. Activity-dependent shedding of the NMDA receptor glycine binding site by matrix metalloproteinase 3: a PUTATIVE mechanism of postsynaptic plasticity. PLoS One 2008; 3:2681; PMID:18629001; http://dx.doi.org/10.1371/journal.pone.0002681.

©2010 Landes Bioscience. Do not distribute

36. Rangaraju S, Khoo KK, Feng ZP, Crossley G, Nugent D, Khaytin I, et al. Potassium channel modulation by a toxin domain in matrix metalloprotease 23. J Biol Chem 2010; 285:9124-36; PMID:19965868; http://dx.doi.org/10.1074/jbc.M109.071266.
37. Craven KB, Zagotta WN. CNG and HCN channels: two peas, one pod. Annu Rev Physiol 2006; 68:375-401; PMID:16460277; http://dx.doi.org/10.1146/annurev.physiol.68.040104.134728.
38. Pifferi S, Boccaccio A, Menini A. Cyclic nucleotide-gated ion channels in sensory transduction. FEBS Lett 2006; 580:2853-9; PMID:16631748; http://dx.doi.org/10.1016/j.febslet.2006.03.086.
39. Garcia-Caballero A, Ishmael SS, Dang Y, Gillie D, Bond JS, Milgram SL, et al. Activation of the epithelial sodium channel by the metalloprotease meprin β-subunit. Channels (Austin) 2011; 5:14-22; PMID:20953144; http://dx.doi.org/10.4161/chan.5.1.13759.
40. Bright SR, Rich ED, Varnum MD. Regulation of human cone cyclic nucleotide-gated channels by endogenous phospholipids and exogenously applied phosphatidylinositol-3,4,5-trisphosphate. Mol Pharmacol 2007; 71:176-83; PMID:17018579; http://dx.doi.org/10.1124/mol.106.026401.
41. Okada Y, Nagase H, Harris ED Jr. A metalloproteinase from human rheumatoid synovial fibroblasts that digests connective tissue matrix components. Purification and characterization. J Biol Chem 1986; 261:14245-55; PMID:3095317.
42. Michaluk P, Mikasova L, Groc L, Frischknecht R, Choquet D, Kaczmarek L. Matrix metalloproteinase-9 controls NMDA receptor surface diffusion through integrin beta1 signaling. J Neurosci 2009; 29:6007-12; PMID:19420267; http://dx.doi.org/10.1523/JNEUROSCI.5346-08.2009.
43. Conant K, Lonskaya I, Szklarczyk A, Krall C, Steiner J, Maguire-Zeiss K, et al. Methamphetamine-associated cleavage of the synaptic adhesion molecule intercellular adhesion molecule-5. J Neurochem 2011; 118:521-32; PMID:21166806; http://dx.doi.org/10.1111/j.1471-4159.2010.07153.x.
44. Puente XS, Sánchez LM, Overall CM, López-Otín C. Human and mouse proteases: a comparative genomic approach. Nat Rev Genet 2003; 4:544-58; PMID:12838346; http://dx.doi.org/10.1038/nrg1111.
45. Liu C, Varnum MD. Functional consequences of progressive cone dystrophy-associated mutations in the human cone photoreceptor cyclic nucleotide-gated channel CNGA3 subunit. Am J Physiol Cell Physiol 2005; 289:187-98; PMID:15743887; http://dx.doi.org/10.1152/ajpcell.00490.2004.
46. Faillace MP, Bernabeu RO, Korenbrot JI. Cellular processing of cone photoreceptor cyclic GMP-gated ion channels: a role for the S4 structural motif. J Biol Chem 2004; 279:22643-53; PMID:15024024; http://dx.doi.org/10.1074/jbc.M400035200.
47. Pugh EN Jr, Lamb TD. Amplification and kinetics of the activation steps in phototransduction. Biochim Biophys Acta 1993; 1141:111-49; PMID:8382952; http://dx.doi.org/10.1016/0005-2728(93)90038-H.
48. Kaupp UB, Niidome T, Tanabe T, Terada S, Bönigk W, Stühmer W, et al. Primary structure and functional expression from complementary DNA of the rod photoreceptor cyclic GMP-gated channel. Nature 1989; 342:762-6; PMID:2481236; http://dx.doi.org/10.1038/342762a0.
49. Chen TY, Peng YW, Dhallan RS, Ahamed B, Reed RR, Yau KW. A new subunit of the cyclic nucleotide-gated cation channel in retinal rods. Nature 1993; 362:764-7; PMID:7682292; http://dx.doi.org/10.1038/362764a0.
50. Chen TY, Illing M, Molday LL, Hsu YT, Yau KW, Molday RS. Subunit 2 (or beta) of retinal rod cGMP-gated cation channel is a component of the 240-kDa channel-associated protein and mediates Ca(2+)-calmodulin modulation. Proc Natl Acad Sci USA 1994; 91:11757-61; PMID:7526403; http://dx.doi.org/10.1073/pnas.91.24.11757.
51. Körschen HG, Illing M, Seifert R, Sesti F, Williams A, Gotzes S, et al. A 240 kDa protein represents the complete beta subunit of the cyclic nucleotide-gated channel from rod photoreceptor. Neuron 1995; 15:627-36; PMID:7546742; http://dx.doi.org/10.1016/0896-6273(95)90151-5.
52. Molokanova E, Trivedi B, Savchenko A, Kramer RH. Modulation of rod photoreceptor cyclic nucleotide-gated channels by tyrosine phosphorylation. J Neurosci 1997; 17:9068-76; PMID:9364053.
53. Gerstner A, Zong X, Hofmann F, Biel M. Molecular cloning and functional characterization of a new modulatory cyclic nucleotide-gated channel subunit from mouse retina. J Neurosci 2000; 20:1324-32; PMID:10662822.
54. Zhong H, Molday LL, Molday RS, Yau KW. The heteromeric cyclic nucleotide-gated channel adopts a 3A:1B stoichiometry. Nature 2002; 420:193-8; PMID:12432397; http://dx.doi.org/10.1038/nature01201.
55. Weitz D, Ficek N, Kremmer E, Bauer PJ, Kaupp UB. Subunit stoichiometry of the CNG channel of rod photoreceptors. Neuron 2002; 36:881-9; PMID:12467591; http://dx.doi.org/10.1016/S0896-6273(02)01098-X.
56. Zheng J, Trudeau MC, Zagotta WN. Rod cyclic nucleotide-gated channels have a stoichiometry of three CNGA1 subunits and one CNGB1 subunit. Neuron 2002; 36:891-6; PMID:12467592; http://dx.doi.org/10.1016/S0896-6273(02)01099-1.
57. Peng C, Rich ED, Varnum MD. Subunit configuration of heteromeric cone cyclic nucleotide-gated channels. Neuron 2004; 42:401-10; PMID:15134637; http://dx.doi.org/10.1016/S0896-6273(04)00225-9.
58. Haynes LW, Kay AR, Yau KW. Single cyclic GMP-activated channel activity in excised patches of rod outer segment membrane. Nature 1986; 321:66-70; PMID:2422558; http://dx.doi.org/10.1038/321066a0.
59. Newman KM, Ogata Y, Malon AM, Irizarry E, Gandhi RH, Nagase H, et al. Identification of matrix metalloproteinases 3 (stromelysin-1) and 9 (gelatinase B) in abdominal aortic aneurysm. Arterioscler Thromb 1994; 14:1315-20; PMID:8049193; http://dx.doi.org/10.1161/01.ATV.14.8.1315.
60. Woessner JF, Nagase H. Matrix Metalloproteinases and TIMPs. Oxford University Press USA 2000; 2.
61. Conant K, Wang Y, Szklarczyk A, Dudak A, Mattson MP, Lim ST. Matrix metalloproteinase-dependent shedding of intercellular adhesion molecule-5 occurs with long-term potentiation. Neuroscience 2010; 166:508-21; PMID:20045450; http://dx.doi.org/10.1016/j.neuroscience.2009.12.061.
62. Molokanova E, Maddox F, Luetje CW, Kramer RH. Activity-dependent modulation of rod photoreceptor cyclic nucleotide-gated channels mediated by phosphorylation of a specific tyrosine residue. J Neurosci 1999; 19:4786-95; PMID:10366613.
63. Gordon SE, Oakley JC, Varnum MD, Zagotta WN. Altered ligand specificity by protonation in the ligand binding domain of cyclic nucleotide-gated channels. Biochemistry 1996; 35:3994-4001; PMID:8672432; http://dx.doi.org/10.1021/bi952607b.
64. Ruiz M, Brown RL, He Y, Haley TL, Karpen JW. The single-channel dose-response relation is consistently steep for rod cyclic nucleotide-gated channels: implications for the interpretation of macroscopic dose-response relations. Biochemistry 1999; 38:10642-8; PMID:10451358; http://dx.doi.org/10.1021/bi990532w.
65. Kleyman TR, Carattino MD, Hughey RP. ENaC at the cutting edge: regulation of epithelial sodium channels by proteases. J Biol Chem 2009; 284:20447-51; PMID:19401469; http://dx.doi.org/10.1074/jbc.R800083200.
66. Kitamura K, Tomita K. Regulation of renal sodium handling through the interaction between serine proteases and serine protease inhibitors. Clin Exp Nephrol 2010; 14:405-10; PMID:20535627; http://dx.doi.org/10.1007/s10157-010-0299-7.
67. Jones BE, Moshyedi P, Gallo S, Tombran-Tink J, Arand G, Reid DA, et al. Characterization and novel activation of 72-kDa metalloproteinase in retinal interphotoreceptor matrix and Y-79 cell culture medium. Exp Eye Res 1994; 59:257-69; PMID:7821370; http://dx.doi.org/10.1006/exer.1994.1107.
68. Ko GY, Ko ML, Dryer SE. Developmental expression of retinal cone cGMP-gated channels: evidence for rapid turnover and trophic regulation. J Neurosci 2001; 21:221-9; PMID:11150339.
69. Ko GYP, Ko ML, Dryer SE. Circadian Regulation of cGMP-Gated Cationic Channels of Chick Retinal Cones. Neuron 2001; 29:255-66; PMID:11182096; http://dx.doi.org/10.1016/S0896-6273(01)00195-7.
70. Paquet-Durand F, Beck S, Michalakis S, Goldmann T, Huber G, Mühlfriedel R, et al. A key role for cyclic nucleotide gated (CNG) channels in cGMP-related retinitis pigmentosa. Hum Mol Genet 2011; 20:941-7; PMID:21149284; http://dx.doi.org/10.1093/hmg/ddq539.
71. Huang SH, Pittler SJ, Huang X, Oliveira L, Berson EL, Dryja TP. Autosomal recessive retinitis pigmentosa caused by mutations in the alpha subunit of rod cGMP phosphodiesterase. Nat Genet 1995; 11:468-71; PMID:7493036; http://dx.doi.org/10.1038/ng1295-468.
72. Payne AM, Downes SM, Bessant DA, Taylor R, Holder GE, Warren MJ, et al. A mutation in guanylate cyclase activator 1A (GUCA1A) in an autosomal dominant cone dystrophy pedigree mapping to a new locus on chromosome 6p21.1. Hum Mol Genet 1998; 7:273-7; PMID:9425234; http://dx.doi.org/10.1093/hmg/7.2.273.
73. Biel M, Michalakis S. Function and dysfunction of CNG channels: insights from channelopathies and mouse models. Mol Neurobiol 2007; 35:266-77; PMID:17917115; http://dx.doi.org/10.1007/s12035-007-0025-y.
74. Fox DA, Poblenz AT, He L. Calcium overload triggers rod photoreceptor apoptotic cell death in chemical-induced and inherited retinal degenerations. Ann NY Acad Sci 1999; 893:282-5; PMID:10672249; http://dx.doi.org/10.1111/j.1749-6632.1999.tb07837.x.
75. Yu WP, Grunwald ME, Yau KW. Molecular cloning, functional expression and chromosomal localization of a human homolog of the cyclic nucleotide-gated ion channel of retinal cone photoreceptors. FEBS Lett 1996; 393:211-5; PMID:8814292; http://dx.doi.org/10.1016/0014-5793(96)00889-7.
76. Peng C, Rich ED, Thor CA, Varnum MD. Functionally important calmodulin-binding sites in both NH_2- and COOH-terminal regions of the cone photoreceptor cyclic nucleotide-gated channel CNGB3 subunit. J Biol Chem 2003; 278:24617-23; PMID:12730238; http://dx.doi.org/10.1074/jbc.M301699200.
77. Schoenmakers TJ, Visser GJ, Flik G, Theuvenet AP. CHELATOR: an improved method for computing metal ion concentrations in physiological solutions. Biotechniques 1992; 12:870-4; PMID:1642895.
78. Gordon SE, Zagotta WN. Localization of regions affecting an allosteric transition in cyclic nucleotide-activated channels. Neuron 1995; 14:857-64; PMID:7536427; http://dx.doi.org/10.1016/0896-6273(95)90229-5.
79. Varnum MD, Black KD, Zagotta WN. Molecular mechanism for ligand discrimination of cyclic nucleotide-gated channels. Neuron 1995; 15:619-25; PMID:7546741; http://dx.doi.org/10.1016/0896-6273(95)90150-7.
80. Fodor AA, Gordon SE, Zagotta WN. Mechanism of tetracaine block of cyclic nucleotide-gated channels. J Gen Physiol 1997; 109:3-14; PMID:8997661; http://dx.doi.org/10.1085/jgp.109.1.3.

©2012 Landes Bioscience. Do not distribute

81. Li J, Zagotta WN, Lester HA. Cyclic nucleotide-gated channels: structural basis of ligand efficacy and allosteric modulation. Q Rev Biophys 1997; 30:177-93; PMID:9293605; http://dx.doi.org/10.1017/S0033583597003326.
82. Molday RS, Molday LL, Dosé A, Clark-Lewis I, Illing M, Cook NJ, et al. The cGMP-gated channel of the rod photoreceptor cell characterization and orientation of the amino terminus. J Biol Chem 1991; 266:21917-22; PMID:1718987.
83. Holm S. A simple sequentially rejective multiple test proceedure. Scand J Stat 1979; 6:65-70.
84. Sakmann B, Neher E. Single-Channel Recording. Springer 1995; 2.

© 2012 Landes Bioscience.
Do not distribute.